DETECTION OF SPECIAL NUCLEAR MATERIAL WITH HIGH PURITY GERMANIUM (HPGe) AND MERCURIC IODIDE (HgI_2) GAMMA DETECTORS

THESIS

Michael B. Nelson, Major, USA

AFIT/GNE/ENP/03-07

DEPARTMENT OF THE AIR FORCE
AIR UNIVERSITY

AIR FORCE INSTITUTE OF TECHNOLOGY

Wright-Patterson Air Force Base, Ohio

AFIT/GNE/ENP/03-07

DETECTION OF SPECIAL NUCLEAR MATERIAL WITH HIGH PURITY GERMANIUM (HPGe) AND MERCURIC IODIDE (HgI_2) GAMMA DETECTORS

THESIS

Presented to the Faculty

Department of Engineering Physics

Graduate School of Engineering and Management

Air Force Institute of Technology

Air University

Air Education and Training Command

In Partial Fulfillment of the Requirements for the

Degree of Master of Science in Nuclear Engineering

Michael B. Nelson, BS

Major, USA

March 2003

AFIT/GNE/ENP/03-07

DETECTION OF SPECIAL NUCLEAR MATERIAL WITH HIGH PURITY GERMANIUM (HPGe) AND MERCURIC IODIDE (HgI_2) GAMMA DETECTORS

Michael B. Nelson, B.S.
Major, USA

Approved:

Larry W. Burggraf (Chairman) — 11 Mar 2003 date

Karen L. Hirsch (Member) — 11 March 2003 date

James C. Petrosky (Member) — 11 MAR 03 date

George John (Member) — 11 March 2003 date

Acknowledgments

"I can do everything through Him who gives me strength." Philippians 4:13

I want to thank my wife and children for being there and supporting me throughout the pursuit of this master's degree. I could not have done it without them.

I would like to express my appreciation to my faculty advisor, Dr. Larry Burggraf, for his guidance in trying to keep me on the correct path throughout this project. I would also like to thank my committee members LTC Petrosky, Dr. John and Dr. Hirsch for their input and guidance. I owe thanks to my sponsor, LTC Cartledge, from the Defense Threat Reduction Agency, for giving the seminar that got me interested in radiation detection and providing much needed assistance.

I am also indebted to the many directors and technicians who helped: Mr. Taylor from the Nuclear Physics Department, Mr. Hastings, Mr. LeValley, and Mr. Inman from the AFIT model shop, Mr. Anderson from the Aeronautics and Astronautics Department, Mr. Anthony and Mr. Wilmoth from the Radiation Safety Office, and the detector experts from Constellation Technology Corporation. Without their assistance, the project would have ended before it began.

Michael Brent Nelson

Table of Contents

Page

Page

Page

List of Figures

Figure **Page**

Figure **Page**

Figure **Page**

Figure **Page**

List of Tables

Table **Page**

Table **Page**

Abstract

The Defense Threat Reduction Agency (DTRA) contracted for two gamma radiation detectors: mercuric iodide (HgI_2) and electromechanically cooled (EMC) high purity germanium (HPGe) to support arms control inspection efforts. This project investigated whether these detectors could measure the quality and quantity of special nuclear material (SNM), particularly Pu-239 for the treaty verification mission. The project investigated two areas of detector capabilities: 1) HgI_2 and HPGe detector performance necessary to characterize the quality of plutonium and the presence of shielding materials and 2) HgI_2 and EMC HPGe detector performance degradation by high noise levels and EMC HPGe detector performance degradation caused by electromechanical-cooling. The first area studied the response functions of each of the detectors necessary to meet the detection objectives: measure the Pu-239/Pu 240 ratio to identify weapons grade plutonium and to identify a phony weapon. The second area of detector performance evaluated was the EMC HPGe detector's cooling capabilities and its effect on the performance of the detector. The results show that neither of the detectors was ideally capable of supporting DTRA's requirements. The HgI_2 detector did not have sufficient efficiency or resolution to distinguish between Weapon Grade and Reactor Grade Plutonium. The EMC system suffered from grounding problems that degraded the resolution and efficiency. An initial study, evaluating the ability of detectors to determine

the presence of a simulated tamper within the SNM physics package, showed great promise for identifying phony weapons.

DETECTION OF SPECIAL NUCLEAR MATERIAL WITH HIGH PURITY GERMANIUM (HPGe) AND MERCURIC IODIDE (HgI_2) GAMMA DETECTORS

I. Introduction

General Issues

Nuclear detection for counter-proliferation and treaty verification requires accurate detection of low levels of radiation from nuclear isotopes. Recent events throughout the world reinforce the need to detect and account for special nuclear materials (SNM). The fear of missing nuclear weapons in the possession of rogue states or terrorists emphasizes the importance of maintaining accountability of the existing nuclear stockpiles. Treaties between the United States and countries of the former Soviet Union require the ability for both parties to be confident that the other is complying with the terms of the treaty. These conditions necessitate sensitive and accurate systems for determining the presence and quality of SNM in a nuclear weapon.

The United States and Russia recently signed a strategic arms control treaty called the Strategic Offensive Reduction Treaty (SORT). SORT further reduces the number of warheads and strategic delivery systems from START I levels to approximately 2000 warheads (23). Although this treaty establishes no new detection limitations; better equipment, capable of verifying treaty compliance is needed. The Defense Threat Reduction Agency (DTRA) has the mission to monitor and verify treaty compliance for the United States (9:27). Consequently, DTRA is seeking better gamma radiation

detectors that will improve confidence in results obtained during treaty inspections of Russian SNM containers.

Problem

The problem addressed in this project is the determination of the quality and quantity of SNM, particularly Pu-239, in a weapon's physics package using semi-conductor based gamma-radiation detectors. A listing of the SNM elements and isotopes that pertain to this project is shown in Appendix A. Emphasis was placed on the ability of a detector to determine the mass ratio of Pu-239 and Pu-240 in the 645 keV portion of a gamma spectrum because these penetrating gammas are accessible.

Determining the plutonium mass ratios enables a treaty inspection team to differentiate between weapon grade plutonium (WGPu) and reactor grade plutonium (RGPu). There are four gamma-energies of interest in the 640 keV range that directly affect the results: 639.99 keV and 645.9 keV peaks from Pu-239, a 642.35 keV peak from Pu-240, and a 241.47 keV peak from Am-241. The 639.99 keV from Pu-239 is used to determine the amount of Pu-239 in the SNM container, while the 642.35 keV peak from Pu-240 is used to determine the amount of Pu-240. Both the Am-241 energy peak and the 639.99 keV Pu-239 peak can overlap the 642.35 keV peak, making the problem more complex. The Am-241 energy peak increases over time from the decay of Pu-241 causing additional complications by changing the spectrum collected from each physics package from inspection to inspection. The initial amount of Pu-241, and hence Am-241, decreases as the quality of the WGPu improves. Despite the complications discussed above, this portion of the spectrum is used because the gammas are close enough in

energy that they undergo similar scattering and absorption effects as they are emitted from the physics package.

The physics package verification is made more complex by absorbing and scattering materials surrounding the SNM. Absorption decreases peak intensities and result in wider, harder to resolve peaks owing to down scattering of higher energy peaks. Additional levels of absorbing and scattering materials in shipping/storage containers further complicate the problem, emphasizing the need for both efficiency and resolution.

Deconvolving the overlapping energy peaks described above can be readily accomplished using a detector with a full width at half-maximum (FWHM) resolution on the order of 2 keV in the 640 keV range (11:33). The detector used for this purpose is a liquid nitrogen (LN_2) cooled, high purity germanium (HPGe) detector. The use of LN_2 for cooling creates a logistical burden and increases costs associated with the purchase and transport of LN_2 and its ancillary equipment.

Detectors made from sodium iodide, with traces of thallium iodide, (NaI(Tl)) provide the most common alternative to HPGe gamma detectors in circumstances where the use of a LN_2 HPGe detector is not practical. This is because the NaI(Tl) detector can be made small enough to be transportable and operates at room temperature. Although the NaI(Tl) detector has better efficiency than the LN_2 HPGe detector, it has relatively poor resolution. As a result, the NaI(Tl) detector cannot be used to distinguish WGPu and RGPu by means of differentiating isotopic mass ratios.

In order to better address the logistical problems associated with LN_2 and resolution problems associated with NaI(Tl), DTRA contracted for evaluation of an

electromechanically-cooled (EMC) HPGe detector and a room temperature mercuric iodide (HgI_2) detector.

Scope

One goal of this study was to continue work in gamma detection conducted by MAJ Thomas Cartledge in 2001 with a Cadmium Zinc Telluride (CZT) detector in support of SNM identification and verification for DTRA (6:75-6). He obtained a resolution of just over 9 keV at 662 keV with an absolute efficiency of 1.3×10^{-5}. Additional study recommendations were made to extend his research to the identification of spoofs by designing and evaluating a weapon mock-up (6:74-5). Although the results obtained in this project showed promise, neither of the experimental detectors proved to be ideal for DTRA's purposes. Recommendations are made for further research into better weapon mock-up design and studies along with recommendations for further research into improving gamma detection through several methods. Particular focus should be given to Compton spectrometry to improve the detector efficiency without degradation of detector resolution.

Assumptions

Several assumptions were made for this project: the physics package follows the Fetter model (12:267), background radiation is higher in a treaty inspection environment, and that the inspection team will operate under time constraints. The first assumption is that the SNM consists of WGPu as shown in Fetter. Note that this model design is not intended to represent any particular weapon, but is used to model the WGPu gamma

radiation emissions of real weapons. The model allows for studies of the effect of different layers of absorbing and scattering material surrounding the WGPu on gamma emissions. The second assumption is that a higher than natural background environment exists during a weapon inspection because emissions of nearby SNM containers. The estimated gamma flux from the Fetter model is 10.8 γ / (s – cm^2) at the surface of the physics package (12:268-71). This gamma flux emanating from each physics package will increase the background of the container under evaluation. The exact level of increase will vary depending on factors such as SNM container design, number of SNM containers in the immediate area, and the distance from the SNM containers to the detector. The third assumption is that the time to collect spectral information is limited to 15-minutes per container because of the number of SNM containers to be inspected (7).

Limitations

START I and SORT.

START I and SORT provide the authority for each country to inspect the other country's nuclear weapon stockpiles in order to verify treaty compliance. To maintain the secrecy of weapon designs, limitations have been placed on the levels of weapon verification. The inspecting country cannot open warheads or containers to physically verify the presence of the nuclear weapon. Although only neutron detectors are listed as authorized radiation detection equipment, gamma detectors are in use (22). It is worth noting that if spectral information collected that builds confidence, it the inspection results probably reveals classified information (5). As a result, the challenge is to identify

a nuclear weapon of unknown size and shape contained within an unknown surrounding material and not reveal specific nuclear design information.

DoD/DOE Limitations

Detector capabilities differ considerably. For the purposes of treaty verification, the high resolution, good efficiency, LN_2 cooled HPGe detector is the best gamma detector currently in use. Because LN_2 HPGe requires a constant supply of LN_2, the LN_2 HPGe detector is not always practical. The room temperature NaI(Tl) detector, with better efficiency and lower resolution, provides detection capability when an HPGe detector is not practical. DoD/DOE working groups currently favor HPGe detectors for measurements in key/fixed locations and NaI(Tl) in remote locations to save time. This creates a problem because the NaI(Tl) detector's limited ability to verify nuclear materials. Appendix A provides a list of the key gammas for both uranium and plutonium, available for gamma radiation detection, during treaty verification inspections. The gammas with the highest emission rates for Pu-249 are at 160 keV and below, making it an area of consideration for plutonium isotopic ratio calculations. However, a common assumption is that gammas with energy levels below 200 keV will be blocked either through self-absorption within the plutonium or shielding within the weapon and the weapon storage container (6:17). Calculations for gamma attenuation at the 200 keV energy level confirm that less than 4×10^{-17} percent of gammas escape the Fetter model.

Detectors

Two varieties of gamma radiation detectors include active and passive detection systems. An active detection system emits radiation into the source and collects the resulting spectrum. DTRA believes that safety issues (arising from possible fissions from using neutrons) and intrusive issues (involved with disclosure of classified weapon design information) exist with using active detection systems (6:5). Passive systems simply collect radiation emitted from the SNM that is incident on the detector. This project limits experiments to passive detection systems provided by DTRA, specifically HPGe and HgI_2 detectors and their ability to identify and verify SNM, particularly Pu-239, along with some spoof devices.

Order of Presentation

The following chapters examine the testing procedures, provide analyses, and record results. Chapter II describes the background information of the radioactive sources, detection equipment, and the warhead mock-up. Chapter III provides detection evaluation and testing procedures. Chapter IV describes the experiment results and analyses. Chapter V discusses conclusions drawn and recommendations for future study. Appendix A through Appendix I provide supporting calculations, tabulated data, and references used throughout the project.

II. Background

Chapter two contains two sections. The first section covers a review of detection theory, gamma interactions, and detector characteristics for the HPGe and HgI_2 detectors as they apply to this project, and signal to noise ratio (SNR) issues. The second section deals with SNM present in nuclear weapons and the challenges involved with SNM detection.

Section 1

Detection Theory

The principal purpose of this project is to study the ability of a detector to resolve two high-energy plutonium peaks located 3.59 keV apart. The primary aspects of the detector that affect this capability are the efficiency and resolution of the detector. Poor resolution results in very broad photopeaks encompassing numerous energy bins on both sides of the energy bin of interest. Good resolution results in a narrow full energy peak, a large peak-to-Compton ratio, and minimal tailing on the low energy side of the full energy peak. HPGe detectors are expected to have Gaussian shaped photopeaks. The photopeak associated with the HgI_2 detector should have a low energy tail while the high-energy side remains Gaussian shaped (16:113-6).

The primary efficiency, of interest in this project, is intrinsic peak efficiency. Intrinsic peak efficiency can be defined as the number of gamma pulses recorded in a detector divided by the number of gamma incident on the detector during any period; after adjustment for the geometry of the detector is taken into account. The higher this ratio,

the better the efficiency of the detector. Detector efficiency falls off as the energy of the incident gammas increases. The HPGe detectors are expected to have better efficiency than the HgI_2 detector used in the project because of size (16:116-9). HgI_2 has better intrinsic efficiency if size is comparable.

Gamma Interactions

There are three gamma interactions of significance for gamma spectroscopy: photoelectric absorption, Compton scatter, and pair production. Photoelectric absorption interactions dominate for the lower energy gammas (≤ 200-300 keV) while pair production interactions dominate the high-energy gamma interactions (≥ 5 MeV). Compton scatter interactions dominate between these two extremes. Figure 1 depicts the relationship of the three interactions as functions of the absorber material's Z number and the energy of the incident photon.

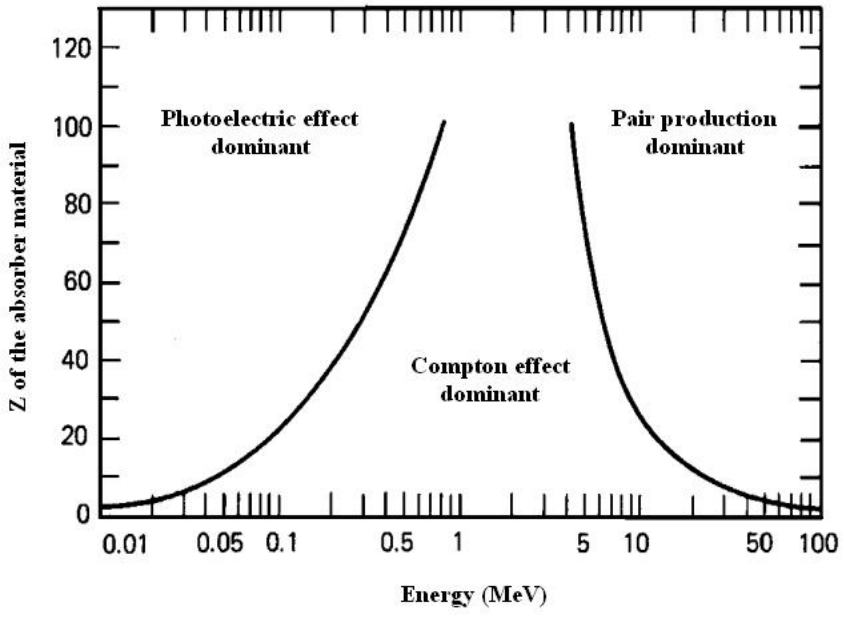

Figure 1 Regions of dominance for gamma interactions within absorbing material (16:52)

Photoelectric absorption results from an interaction in which a bound electron within the detector or absorbing material absorbs the energy from an incident gamma photon. The result of the interaction is a photoelectron with most of the energy of the incident photon. When this interaction occurs entirely within the detector, the result can be measured as the full energy peak or photopeak. The higher the Z value within the absorbing material, the greater the probability of photoelectric absorption. When this interaction occurs in an absorbing material other than the source, it results in a loss of possible full energy peak interactions within the detector and a reduced photopeak efficiency (16:309; 14:24-5).

The Compton scatter process is a result of an incident gamma elastically scattering off an electron. Energy from the scattered gamma and the electron depends on the scattering angle relative to the incident gamma, with the incident energy being divided between the two particles and give rise to the Compton distribution within the resulting spectrum. The photon's scatter angle varies from 0 degrees at low energy to 180 degrees near the photopeak. Energy from the scattered electron is collected at energy levels other than the incident photon energy, causing a reduction in the photopeak-to-Compton ratio. The resulting gamma may escape the detector and be lost altogether (16:310-11; 14:25-6).

Compton scatter events may also occur within material surrounding a source. Under these conditions, the resulting photon from the Compton scatter event may be incident upon the detector. This new photon could be absorbed through photoelectric absorption with a lower energy than the source, or may undergo additional Compton scatter within the detector.

A detector can be considered small when the size of the crystal is smaller than the mean free path of secondary gamma radiation produced from interactions with the incident gamma photon (16:312-3). Higher energy gammas have longer pathlengths making a clear separation between sizes complex. The HgI_2 detector falls into the small detector category because of the physical size of its crystal (1.77 mm thick) when compared to the mean free path of the plutonium peaks in the 640 keV range (3.77 mm) used in treaty verification as well as the 662 keV gammas from the Cs-137 distributed source used throughout this study. The HgI_2 response function is not expected to have Gaussian photopeaks at higher gamma radiation energies owing to the hole tailing and scatter effects within the HgI_2 crystal (14:54-5). This problem should increase at higher energies as the Compton interactions increase in magnitude.

Both of the HPGe detectors used in this project would be considered moderately sized detectors (16:315-7). A moderately sized detector has a large enough crystal that the pathlength of the gammas used in this project will be collected within the crystal as long as the Compton interaction does not occur within a pathlength of the crystal's edge.

Signal to Noise Ratio

The low counts expected in the weapon verification inspections require improvements in the SNR of most detectors. Several methods exist for improving the response function, such as Compton rejection by anti-coincidence (16:437-8) and using a Compton spectrometer (16:324-5).

Using an anticoincidence system will reduce the Compton continuum and improve the SNR in addition to rejecting gamma photons originating from outside the source

(such as cosmic rays or gamma photons from an adjacent SNM container). Anticoincidence uses a guard detector surrounding the primary detection area. The guard detector's purpose is to detect the gamma interaction and not resolve the energy of the interaction. For this reason, the energy resolution of the guard detector is not important (14:251). This method rejects any pulses that occur simultaneously in both the primary detector and the guard detector. A major disadvantage to any of these systems is the reduction in efficiency. This becomes especially important in low-count environments.

The principles of Compton spectrometry can be used to improve the overall efficiency of a two-detector system like the system shown in Figure 2. Incident gammas from a collimated source would strike the first detector and give rise to Compton scatter events. Such a system allows a moderate-resolution detector, such as an HgI_2 or CZT detector, to be used as the first detector. The second detector could be a high efficiency NaI(Tl) detector. The two detectors would be operating in coincidence mode. The energy at which Compton events are collected in the first detector will be lower energy than the incident photons and, as a result, will be measured in a higher efficiency and higher resolution portion of the energy spectrum. Combining the signals from the coincidence Compton spectrometer and the signals from incident energy photopeak results in improved efficiency as long as the collimation required for the Compton spectrometer does not significantly diminish the acceptance solid angle for the first detector. The advantage to this method is that it allows room-temperature detectors, with their logistics and mobility advantages over LN_2 detectors, to have improved efficiency without loss of resolution.

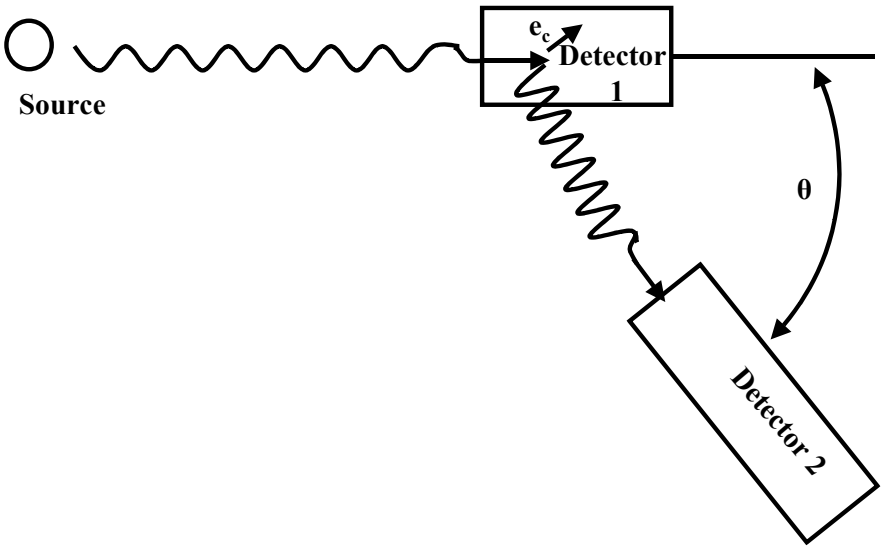

Figure 2 Geometry used in a typical Compton spectrometer configuration for collecting gammas scattered from a 400-600 keV incident source

Detectors

Semiconductor detectors are one of several types of gamma radiation detectors. The advantages of semiconductor based gamma radiation detectors include: higher energy resolution, compact size, relatively fast timing characteristics, and an effective thickness that can be varied to match the application requirements. Disadvantages include size limitations in detectors made from materials such as HgI_2 (advances are being made in this regard as the purity of the crystal is improved) (16:353-4).

The "ideal" detector would have the following characteristics (7):

1) Large active volume to take advantage of increased geometric efficiency and to shorten the counting time.

2) High charge-carrier mobility and long charge-carrier lifetime to improve charge collection.

3) High atomic number detector materials to increase the probability of photoelectric interactions.

4) Relatively small bandgap to reduce the average ionization energy required to produce electron-hole pairs and to increase the number of charge carriers created per unit of deposited energy while maintaining room temperature operation without a cooling apparatus to reduce the logistical requirements of the detector.

A resolution of 2 keV FWHM at 640 keV should be sufficient to distinguish between Pu-239 and Pu-240. Of the detectors listed in Table 1, only the HPGe detector meets most of the requirements listed above and has the required resolution. The remaining detectors shown in Table 1 represent the room temperature alternatives to HPGe. NaI(Tl) is well established and doesn't have the resolution to perform the primary mission for DTRA; but the CZT (6) and the HgI_2 detectors (26) have both shown promise as potential solutions, but they still have problems that must be resolved.

Table 1 Representative radiation detection and measurement systems used by the DTRA (3:3-4)

Detector System	Resolu-tion	Photoelectric Efficiency (% per mm @0.1 and 1.0 MeV)	Practical Efficiency @ 0.1 and 1.0 MeV	Comments	Potential DTRA Application
HPGe cooled to ≈ 77 K	≈ 0.2%	18.0 0.041	High; moderate	Best available charge collector for High-resolu-tion spectros-copy; require LN_2 or EMC; useful range: a few keV to several MeV	Radionuclide spectral analysis for nonprolifera-tion/ nuclear activities, WGPu detection
HgI_2 (room temp)	2 - 10%	65.5 0.58	high; very high	Potential for very high efficiency; available thickness (≈ 2 mm) limits high-energy efficiency; useful range: few keV to several MeV	Field use, nonprolifera-tion, detecting Pu, possibly U.
CZT	3 - 10%	52.3 0.21	high; moderate	Degraded resol-ution at room temp; compact; available thickness limits high-energy resolution	Nonprolifera-tion, field use, Pu detection. Warhead authentication confirming presence of Pu
NaI(Tl) (room temp)	7 - 10%	34.6 0.13	high; very high	Traditional scintillator for low resolution apps; large sizes, high efficiency; need photo sensing unit; useful range: 10s keV to several MeV	NaI: field use, nonprolifera-tion, detecting Pu, possibly U. Warhead authentication, confirming presence of Pu, possibly of U.

The NaI(Tl) detector's resolution is 7-10 percent of the FWHM at 640 keV. As a result, the scintillation detector is only capable of identifying the existence of plutonium and not the isotopic make-up of the plutonium. Despite this shortfall, it remains the detector of choice when portability is the driving requirement during an inspection and a good choice for use in a Compton spectrometer.

HPGe Detectors

Two HPGe detectors were used during this project. The experimental HPGe detector used in this project was a standard p-type coaxial detector (16:405-54). The EMC HPGe detector is cooled by a Sunpower M77 Stirling cryocooler with an attached, motor-driven active vibration cancellation as a counterbalance (8:12). The detector design allows for a temporary low-power engine setting in order to collect a gamma spectrum with reduced Stirling engine-induced background, leading to improved resolution (8:31). Comparisons were madeof spectra drawn with the cooling power at full power, low power, and with the cryocooler turned off to evaluate the practicality of using the lower power settings during inspections. A LN_2 HPGe detector was used to establish the isotopic properties of the plutonium test sample and was used to test and evaluate the weapon mock-up. The LN_2 HPGe detector was a standard n-type coaxial detector (16:405-54).

HgI_2 Detector

Historically, HgI_2 detectors had several problems to overcome; the most significant of which are hole trapping, low hole mobility, short charge carrier pathlength, and crystal surface degradation (7). Constellation Technology Corporation (Constellation) developed

a high purity synthesis and purification processes that allow single crystals of HgI_2 to be grown up to 25 x 25 mm with cross sections as thick as 3 mm for commercial purposes (24:108). Although the hole-tailing problem associated with incomplete hole collection still exists, resolutions of 3 percent (20 keV) at 662 keV has been recorded by the manufacturer. Research continues to produce crystals as thick as four to five mm to increase photopeak efficiency by increasing the stopping power of the crystal (26:149-50). A larger crystal has inherent problems associated with hole collection. Low energy gammas are stopped near the surface of the crystal and are almost entirely collected in the expected Gaussian shape. The higher energy gammas, which stop deeper inside the larger crystal, have a relatively long charge collection time that results in an increased hole-tailing effect (14:55-6). The larger bandgap and increased stopping power resulting from its higher density make the HgI_2 detector, potentially, the best detector with regard to room temperature operation. Although MAJ Cartledge et al demonstrated that the resolution of CZT is a factor of two better at 662 keV.

Section 2

Special Nuclear Material

The signature isotopes for SNM include U-235, U-238, Pu-239, and Pu-240. The primary SNMs of interest are fissile materials, U-235 and Pu-239. Table 2 lists the isotope mass percentages of plutonium for the three standard classifications (10:A-3). WGPu consists of typical plutonium ratios used in nuclear weapon, hence the name. RGPu plutonium ratios shown are typical values of the mixture of plutonium isotopes at the end of the burn cycle in a pressurized water reactor at a nuclear power plant. Fuel grade is the name given to ratios of plutonium that fall between the two extremes. The mass ratio of Pu-239 to that of Pu-240 is critical to identifying whether the plutonium is WGPu.

Table 2 Isotope mass percents for different plutonium grades applicable to SNM identification

Isotope	238	239	240	241	242
WGPu (SNM)	< 0.0005	0.936	0.06	0.004	< 0.0005
Fuel Grade	0.001	0.861	0.12	0.016	0.002
RGPu/Power Grade	0.100	0.620	0.22	0.120	0.030

Am-241 can also be used as an indication of the grade of plutonium. RGPu has 30 times more Pu-241 than WGPu. This difference in Pu-241 causes an proportional increase in the daughter element, Am-241. The differences in Am-241 levels become more obvious over time as the Pu-241 decays.

SNM Detection Challenge

An inspection team attempts to determine which of three possibilities exist within a warhead or SNM container: an actual warhead/component, an intentional fake (*spoofing* device), or an empty container as shown in Figure 3.

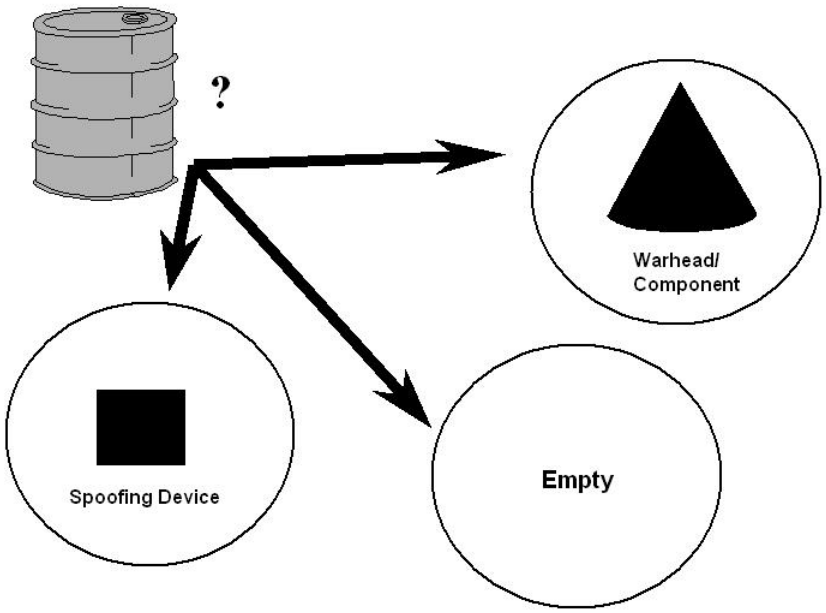

Figure 3 Environmental challenges to SNM verification of the contents of a closed container

While the SNM is shielded, the inspectors must make a determination of the existence or non-existence of the SNM. Identification of an empty container is a simple task for any of the detectors used by inspection teams owing to the lack of a gamma radiation signature. The challenge is in determining whether the container holds a legitimate warhead or a spoofing device.

The determination of legitimate SNM is challenging under ideal circumstances. Several layers of scattering and absorbing materials surround stored SNM making the determination of SNM more difficult. Some shielding protects personnel in the vicinity of the SNM container. This shielding is in addition to significant levels of self-shielding because of the dense material of which SNM is composed. There will be additional shielding from the weapon's casing and container. This shielding absorbs lower energy gammas and attenuates higher energy gammas that scatter through secondary Compton interactions. This multiple scattering can register as noise at lower energies to the detector.

Materials, such as paraffin, are used because they have low atomic number and high hydrogen density to moderate and absorb neutrons emitted from the source. A consequence of the neutron capture by hydrogen is a high-energy gamma of approximately 2 MeV (21:6-5). This high-energy gamma can scatter and be absorbed within the warhead or nuclear weapon. The gamma can also scatter from the warhead or nuclear weapon at a reduced energy owing to Compton interactions and get captured within the detector. This captured gamma adds to the background spectra.

The attenuation of the gammas can be calculated using the appropriate cross section values, examples of which are shown in Appendix B. The attenuation coefficients are used to calculate the percentage of the gammas emitted by the source that pass unaltered through the absorbing and scattering materials surrounding the SNM. Gammas can scatter into the detector in addition to scattering outward. A build-up factor increased counts, within the detector response function, because of gammas scattering into the detector.

Plutonium isotope ratios are complex to identify. The plutonium with the highest gamma decay rate, five percent, is easily attenuated 13.6 keV x-rays. The remaining plutonium gammas of interest occur less than 0.03 percent of the time (Table 12 and Table 13). Plutonium has additional gamma peaks useful to differentiate between WGPu and RGPu in the 640 keV range that were described earlier.

The fact that an inspected party may try to create a spoof causes concern. In order to investigate a gamma radiation detector's ability to identify a spoof, a weapon mock-up was created based upon the model shown in Figure 4 (12:267).

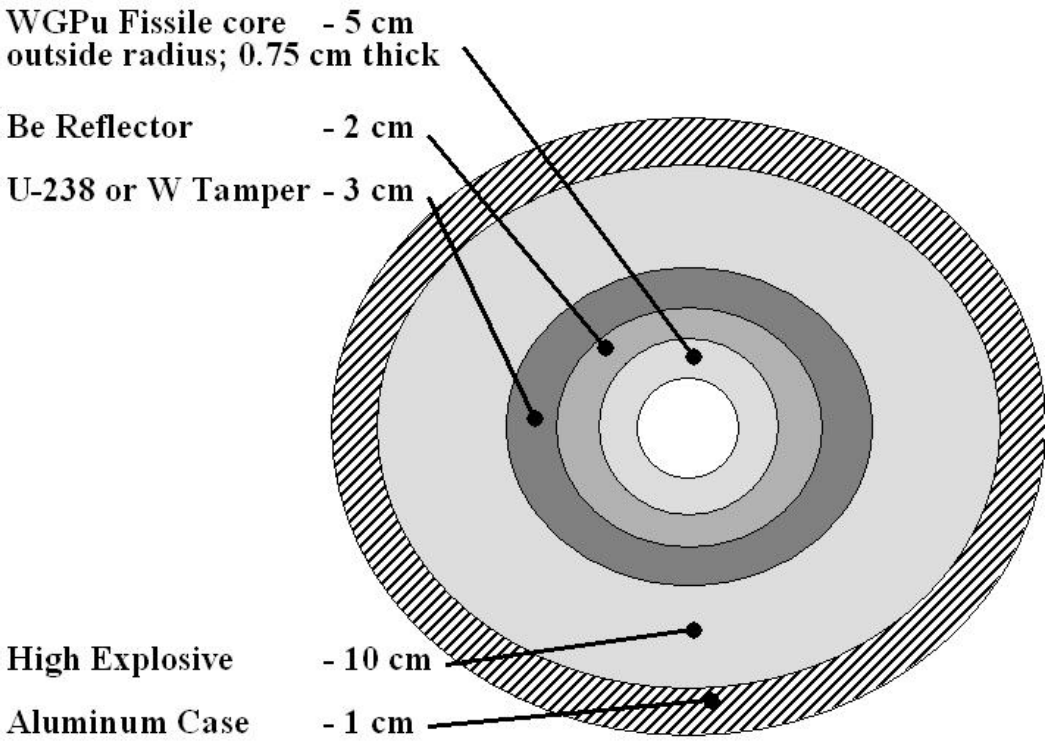

Figure 4 Hypothetical weapon model of a physics package used in this project

Reducing the amount of SNM or exchanging the WGPu with RGPu creates one type of spoof. The reduced amount of SNM spoof requires the reduction or removal of scattering material within the physics package to maintain the correct intensity of gamma emissions on the surface of the container. This type of spoof may be identified by a combination of spectroscopy measurements that record the changes caused by the missing scattering material. The combination of spectroscopy measurements may be used because the Pu-239 intensities at the 400 keV range differ from Pu-239 intensities in the 640 keV range. This results from the photoelectric absorption changes according to the formula

$$\tau = k * \frac{Z^{4.5}}{E^{3.5}}, \tag{1}$$

where τ is the photoelectric absorption per atom, k is a proportionality constant, Z is the Z value of the absorbing material, and E is the gamma energy in keV. Careful creation of a spoof to maintain the correct 640 keV energy intensity will result in a detectable change in the 400 keV range of the gamma spectrum.

This project will focus on direct identification of the missing scattering material based on the mock-up shown in Figure 5. The innermost three sections of the Fetter model were used to design the mock-up. The mock-up consists of a polymer hemispherical bowl filled with an aqueous solution of Cs-137 source acidified with 1 M HCl, a hollow aluminum hemispherical shell filled with water, and a solid lead hemispherical shell. Details of the mock-up constructed can be found in Appendix C.

Figure 5 Components of a weapon mock-up consisted of an inner polymer bowl containing a distributed source, a simulated reflector made of spun aluminum filled with water, and a simulated lead tamper on the outside

III. Methodology

This chapter provides the methodology for the spectral testing of the EMC HPGe and the HgI_2 detectors. Additionally, this chapter provides the methodology for testing the EMC HPGe detector's different cooling modes: normal cooling, reduced cooling, and temporary cooling shutoff. The chapter includes methodology for the evaluation of the follow-on work in spoof identification.

Test Objectives

Several experiments were performed to investigate the detection abilities of the two detectors: EMC HPGe, and HgI_2. Areas of interest include detection and identification of WGPu spectrum. In addition, particular emphasis was placed on identifying a potential spoofing device by analysis of the full energy peak and Compton scatter spectrum. Experiment results were used to answer the following questions:

1. For the room temperature detector, can the HgI_2 detector be used not only to detect SNM, but also identify the grade of the SNM in question?

2. For the cooled detector, can the EMC HPGe detector be used as a replacement for the LN_2 cooled HPGe detector standard?

3. What is the resolution degradation of the EMC HPGe detector in each of the two reduced cooling modes?

4. For spoof identification, can a solid-state detector provide spectral data for identification of a spoofing device resulting from replacing WGPu with RGPu or reducing the amount of SNM and removing the tamper?

Characterize Detectors

The basic steps involved in detector characterization include energy calibration and efficiency calibration. Standard gamma point sources were used to perform these calibrations. The characterized detectors were used to gather SNM spectral data from both uranium and plutonium sources.

To determine the level of degradation in the resolution of spectral data, the EMC HPGe detector was operated with its Stirling cryocooler in its three cooling modes: normal operating power, reduced power, and no power.

Characterize the Weapon Mock-up

A full description of the mock-up used to simulate a weapon's physics package is presented in Appendix C. Characterization of the simulated weapon mockup required gathering spectral data with the LN_2 HPGe detector for each of the three mock-up configurations. The configurations used were with the source alone, the source covered by the simulated reflector, and the simulated reflector covered by the simulated tamper. Evaluating the different configurations proved critical for investigating any effects of higher energy gammas being scattered into lower energy gammas by either the simulated reflector or the simulated tamper. These tests made it possible to examine features such as peak-to-valley ratio and changes in the valley location for possible clues of a missing tamper.

Description of the Tests

Characterize the Detectors

A known multinuclide gamma source was used to characterize the HgI_2 and the HPGe detectors. Individual point sources were used to check the resolution obtained from the electronics compared to the resolution reported by the detector manufacturer (Constellation). Figure 6 and Figure 8 show the configuration of the respective detection systems for the HgI_2 and EMC HPGe detectors. Figure 7 and Figure 9 show pictures of the HgI_2 and EMC HPGe detectors evaluated. Additional detector information is found in of Appendix F.

Both detectors were used to collect spectra from the multinuclide source. The isotopes included in the multinuclide point source can be found in Appendix D. The geometry used in making approximations for the solid angle subtended by the detectors can be found in Appendix E. The source was placed eight centimeters in front of the face of the HgI_2 detector to improve the efficiency by causing the gammas enter the detector normal to the front face of the crystal. The source was placed 30 cm in front of the face of the EMC HPGe detector to minimize the dead time effects on the detector. Am-241, Co-57, and Cs-137 point sources verified the results of the calibration procedures.

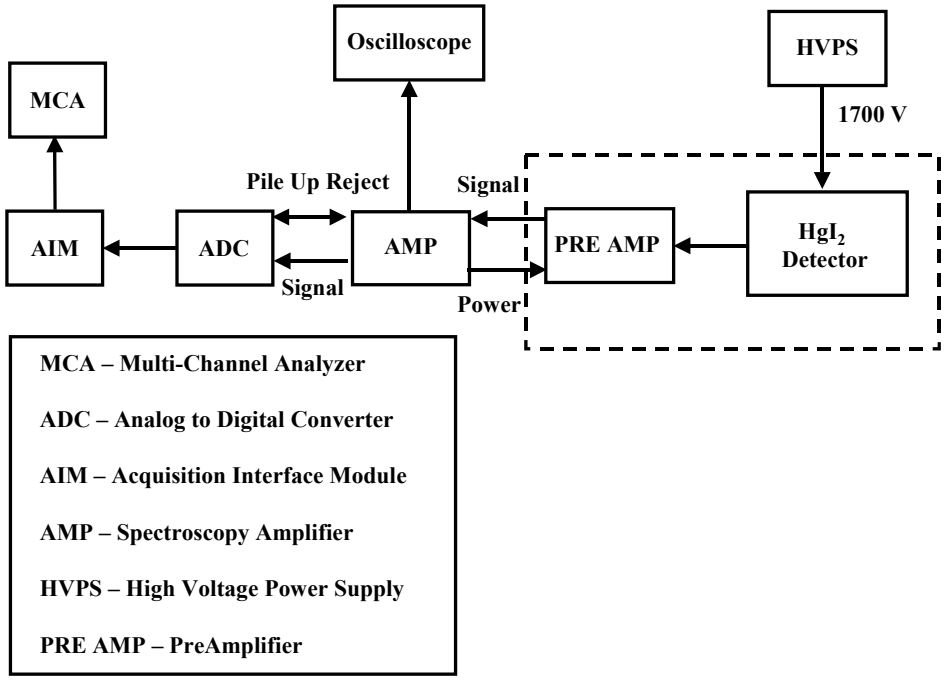

Figure 6 HgI_2 detector electronics configuration

Figure 7 HgI_2 detector evaluated as part of the project

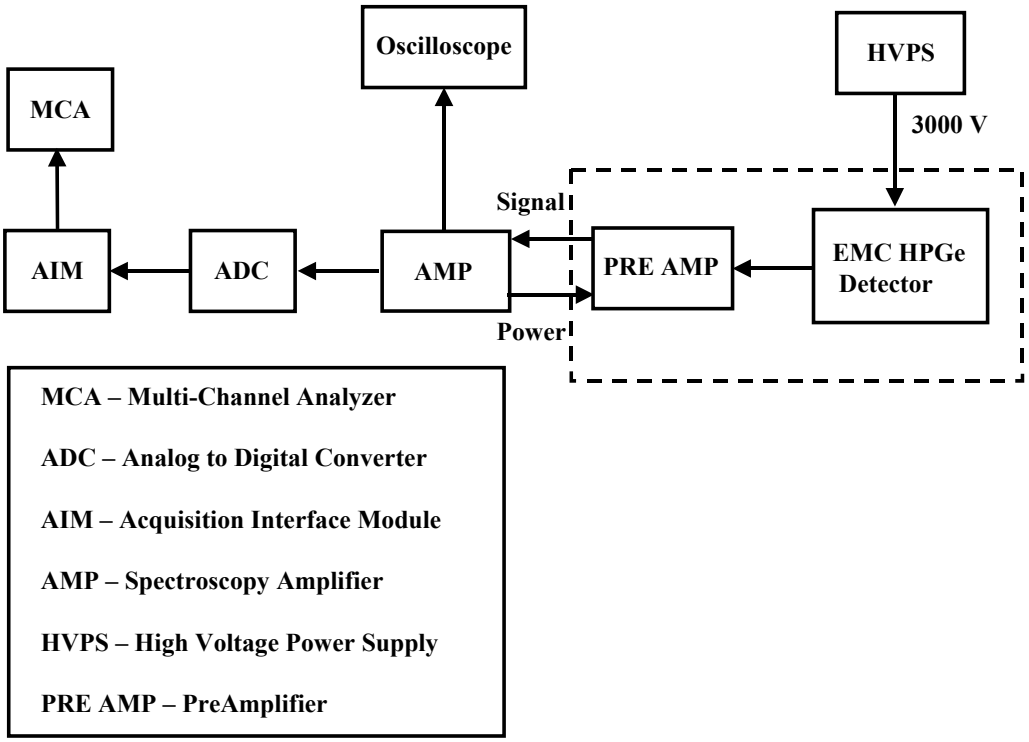

Figure 8 EMC HPGe detector electronics configuration

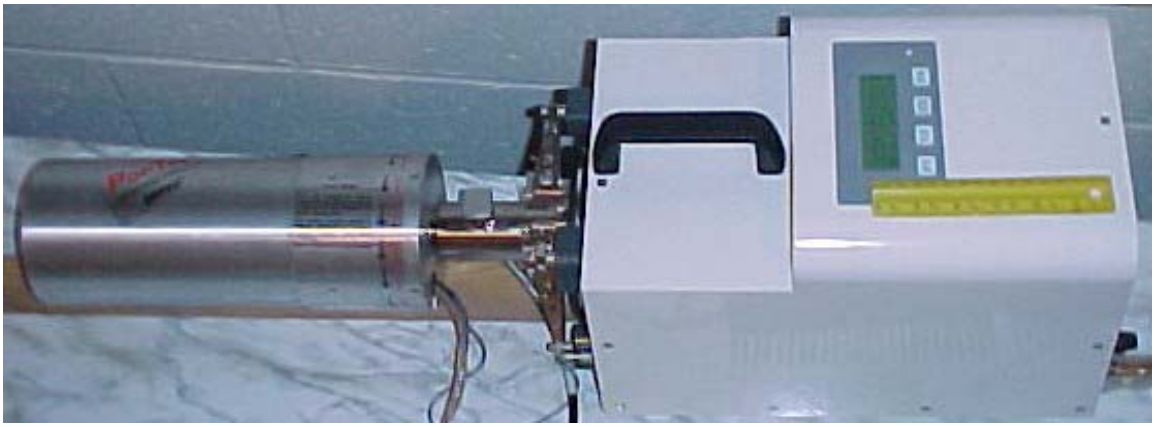

Figure 9 EMC HPGe detector evaluated as part of the project

Characterize the Effects of Cooling Settings on the EMC HPGe Detector

Two experiments were conducted to investigate the effects of the different Stirling engine power settings. For the first experiment, spectral information was collected at the "reduced power setting" and at the "no power setting" for 2, 5 and 15-minutes to determine the resolution degradation under each of the cooling modes. For the second experiment, spectral information was collected several times, with one minute between readings. The results of this experiment show how many SNM containers could be evaluated before the EMC system cycled from regulating mode (normal operating) to cooling mode.

Characterize the SNM Sources

The SNM sources included a natural uranium ore sample and a plutonium source consisting of approximately a plutonium isotope mass ratio of 80 percent Pu-239 to 20 percent Pu-240. Each of the detectors was used to collect spectral data that was analyzed to determine the mass percentage of the uranium isotopes. The same procedure was used to collect information on the plutonium source. Details of both of the SNM sources are in Appendix D.

Characterize the Weapon Mockup

Spectral data was collected under all mock-up configurations: the source by itself, the source covered by the simulated reflector, and the simulated reflector covered by the simulated tamper. In each of these conditions, a two-hour spectrum (live time) was

gathered from a distance of approximately 38 cm, using the LN_2 HPGe detector. Figure 10 shows the configuration of the LN_2 HPGe system used in the project. A description of the mockup and its construction can be found in Appendix C.

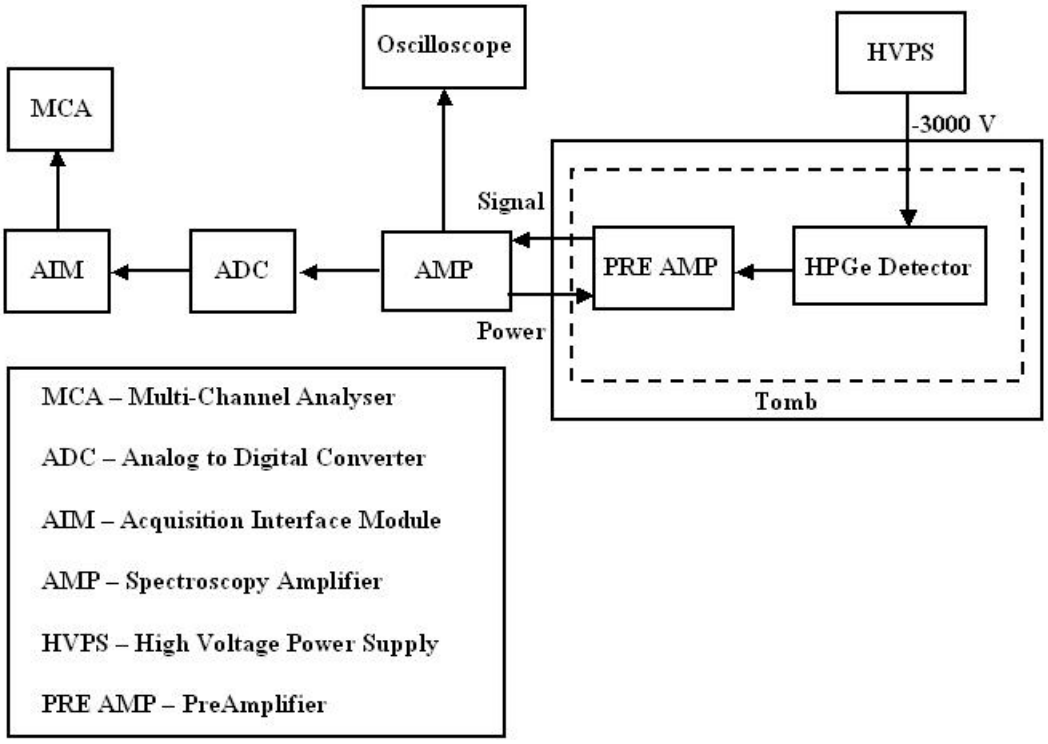

Figure 10 LN_2 HPGe detector configuration used throughout the project

Lead shielding was added around the sides of the LN_2 HPGe detector to minimize the amount of scattered gammas that entered the sides of the coaxial detector. The front face of the detector was left unchanged.

Special Requirements

A listing of equipment and equipment settings used in the experiments can be found in Appendix F. A LeCroy 9410 oscilloscope and a Fluke 77 multimeter were used to test the detection components and systems for proper spectroscopy operation.

The sources used in this project are listed in Appendix D. Additional information about the making of the distributed source used throughout the spoof identification experiment can be found in Appendix G.

IV. Test and Evaluation

A multinuclide source, T105 from Appendix D, was used to calibrate the HgI_2 detector and both HPGe detectors for both energy and efficiency. All detectors were evaluated using configuration shown in Appendix D. The locations of the energy peaks within the spectra were verified with Cs-137, Co-57, and Am-241 point sources from Appendix D. Figure 11, Figure 12, and Figure 13 show the spectrum collected from each of the detectors.

Characterize the Detectors

1) HgI_2 Detector

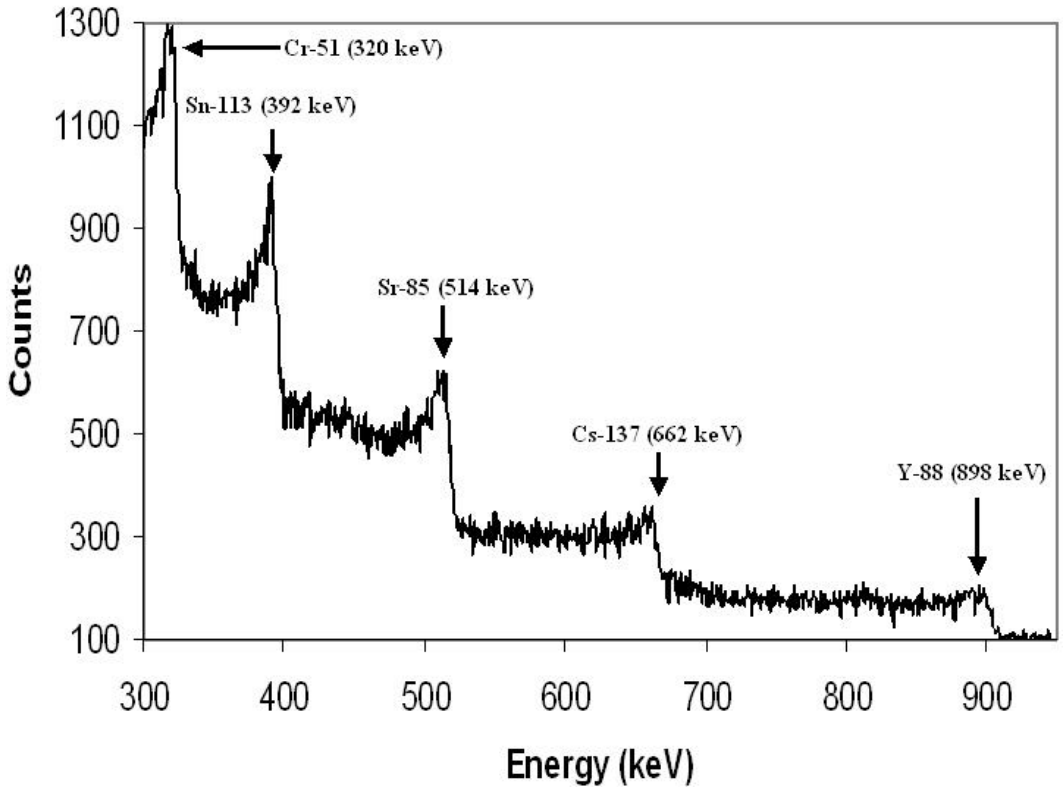

Figure 11 12-Hr multinuclide point source spectrum with the background removed collected 8 cm from the source with the HgI_2 detector

The full energy peaks associated with the HgI_2 detector lost their Gaussian shape with increased energy because of low-energy hole-tailing effects and Compton scatter associated with the small size of the HgI_2 detector. Beginning with the Sr-85 nuclide peak, the low-energy tail and Compton scatter effects became large enough to make peak resolution calculations extremely difficult. From the full energy peak associated with Y-88 and higher energies, the hole tailing effects and Compton scatter in the detector response degraded to such a poor condition that the only clearly identifiable feature remaining in the full energy peak was the upper half of the peak.

Because of the nature of the Genie software, the only detector options were NaI and Ge (13:51). The peak shapes that the default algorithms of the Genie software produced were inadequate for directly evaluating the HgI_2 spectra. Because of this, all resolution calculations were performed by hand. Even making determinations about the low energy point at which to begin counting the energy peak was difficult because of the nearly flat tail response of the low energy tail at higher energies. As a result, the low energy point for the FWHM calculations became a matter of best guess instead of a clearly defined cut-off point.

2) EMC HPGe Detector

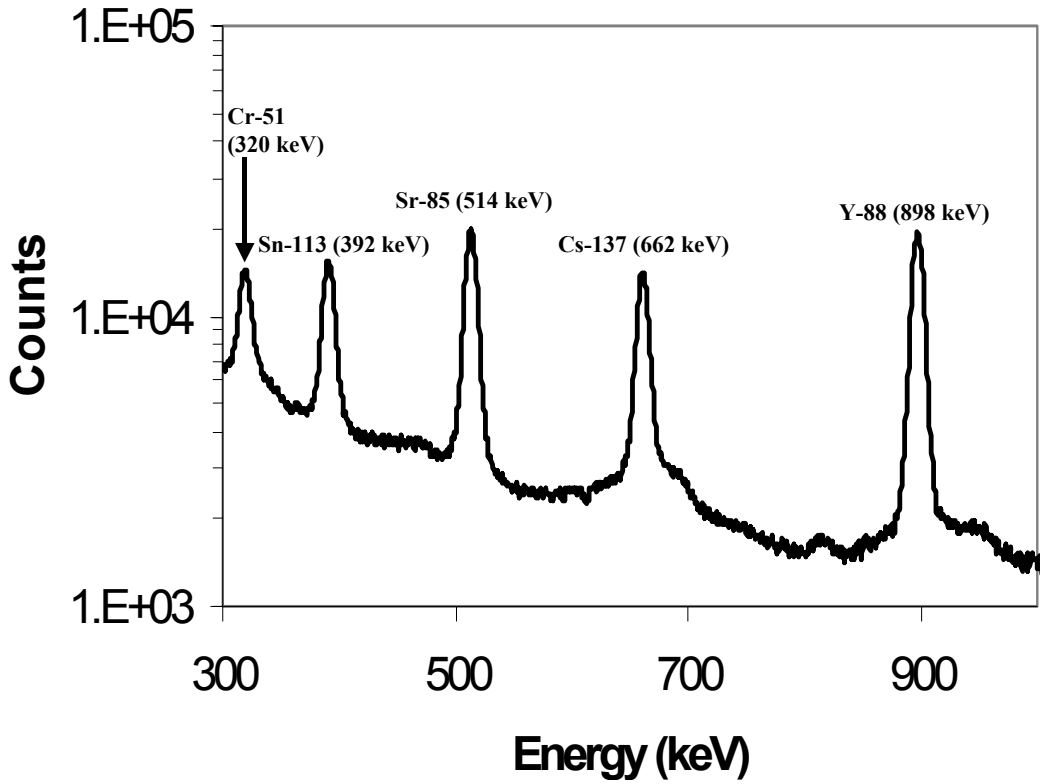

Figure 12 10-hr multinuclide point source spectrum with the background removed collected from 30 cm with the EMC HPGe detector in normal operating conditions

The basic form of the response function of the EMC HPGe detector appeared normal, but closer examination revealed that the FWHM at 662 keV is 11.5 keV. There was clear evidence of low frequency noise; however, this occurred below the 300 keV region. Because of the nature of the cryocooler noise, a higher background was recorded than expected from a typical HPGe detector.

Evidence of normal, natural uranium appeared in the EMC HPGe detector background spectrum. This background was detected because the EMC HPGe detector was not shielded. Careful examination of the HgI_2 detector spectrum indicated that the uranium background was not present. This lack of a uranium background resulted from the smaller and less efficient HgI_2 crystal.

3) Ln2 HPGe Detector

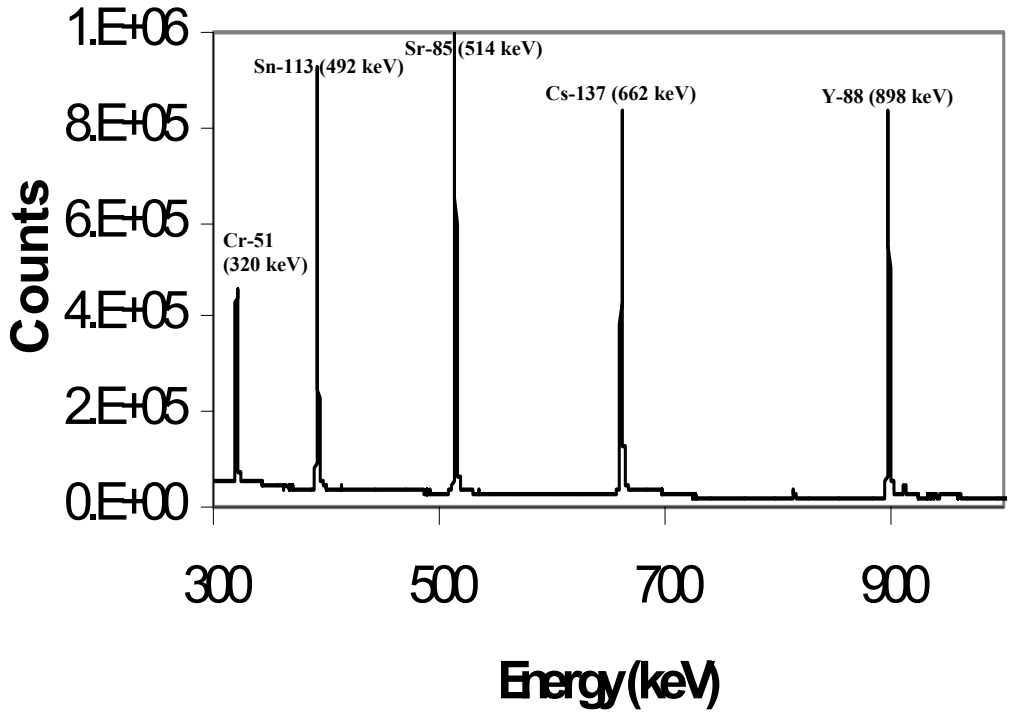

Figure 13 24-hr multinuclide point source spectrum with the background removed collected at a total distance of 0.5 cm with the LN2 HPGe detector

The LN_2 HPGe detector provided the peak shape and efficiency (1.69 keV at 662 keV) expected from a quality detector for spectroscopic purposes in the evaluation of a test sample. The spectrum shown was collected with the source placed directly on the face of the detector.

Characterize the Detectors

Energy and Efficiency Calibration

The Genie 2000 software used designated key gamma energies associated with the gamma peaks in the multinuclide spectra to perform an algebraic fit to convert the channel number to energy. The empirical equations used by each of the detectors for energy and efficiency calibrations are listed below.

1) HgI_2:

$$\text{Energy} = 4.454\ \text{eV} + 0.6846 * (\text{Channel Number}) \quad (2)$$

$$\text{FWHM} = 1.387\ \text{eV} + 0.0387 * \text{Energy}^{1/2} \quad (3)$$

$$\ln(\text{efficiency}) = 1509 - 1474 \ln(\text{Energy}) + 567.2 \ln(\text{Energy})^2 - 107.8 \ln(\text{Energy})^3 + 10.11 \ln(\text{Energy})^4 - 0.3746 \ln(\text{Energy})^5 \quad (4)$$

2) EMC HPGe:

$$\text{Energy} = -1.014\text{eV} + 0.767 * (\text{Channel Number}) \quad (5)$$

$$\text{FWHM} = 1.547\ \text{eV} + 0.04559 * \text{Energy}^{1/2} \quad (6)$$

$$\ln(\text{efficiency}) = -158 + 72.55 \ln(\text{Energy}) - 11.49 \ln(\text{Energy})^2 + 0.5991 \ln(\text{Energy})^3 \quad (7)$$

3) LN_2 HPGe:

$$\text{Energy} = -1.014\text{eV} + * (\text{Channel Number}) \quad (8)$$

$$\text{FWHM} = 1.547\ \text{eV} + 0.04559 * \text{Energy}^{1/2} \quad (9)$$

$$\ln(\text{efficiency}) = -94.95 + 72.38 \ln(\text{Energy}) - 22.02 \ln(\text{Energy})^2 + 3.291 \ln(\text{Energy})^3 - 0.2451 \ln(\text{Energy})^4 + 0.007284 \ln(\text{Energy})^5 \quad (10)$$

Figure 14 through Figure 16 show the efficiency curves obtained from the empirical formulas above of the three detectors as functions of the incident photon energy. The HgI_2 detector intrinsic efficiency at 662 keV was 7.56×10^{-6} while the EMC HPGe detector had efficiency at 662 keV of 6.61×10^{-4}. An efficiency of 1.82×10^{-2} was determined for the LN_2 HPGe detector at 662 keV.

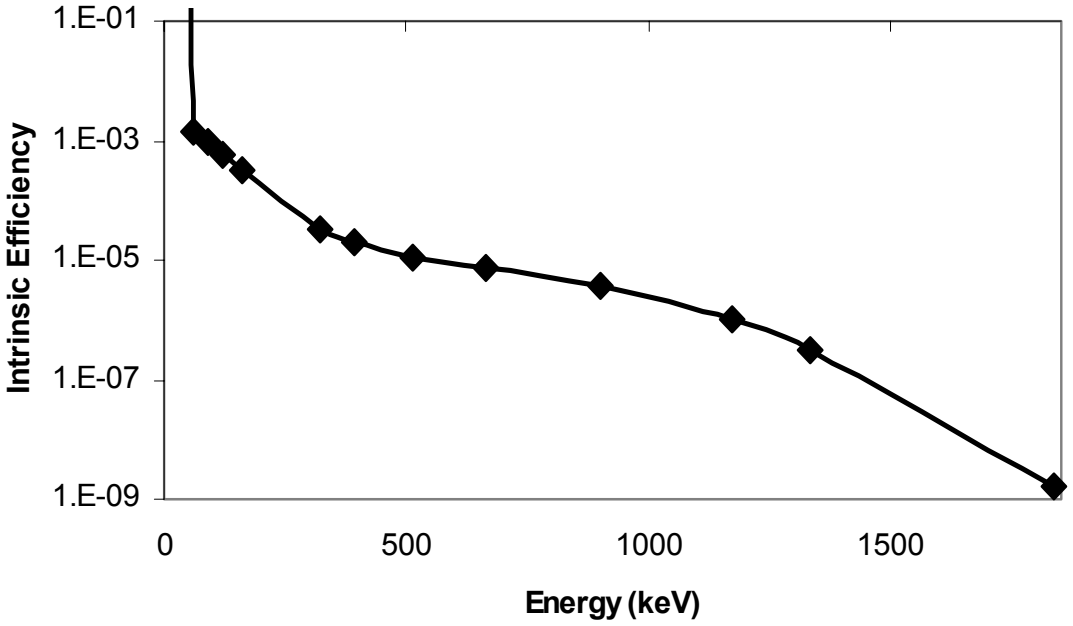

Figure 14 Intrinsic peak efficiency of the HgI_2 detector as a function of incident gamma energy with the source located 8 cm in front of the face of the detector

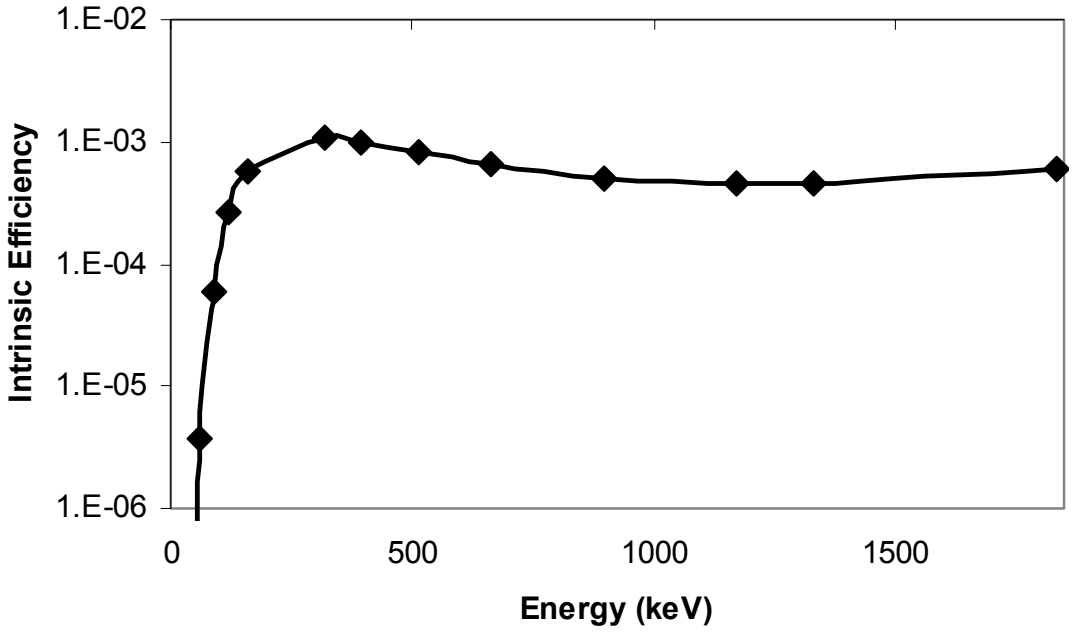

Figure 15 Intrinsic peak efficiency of the EMC HPGe detector as a function of incident gamma energy with the source located 30 cm in front of the face of the detector

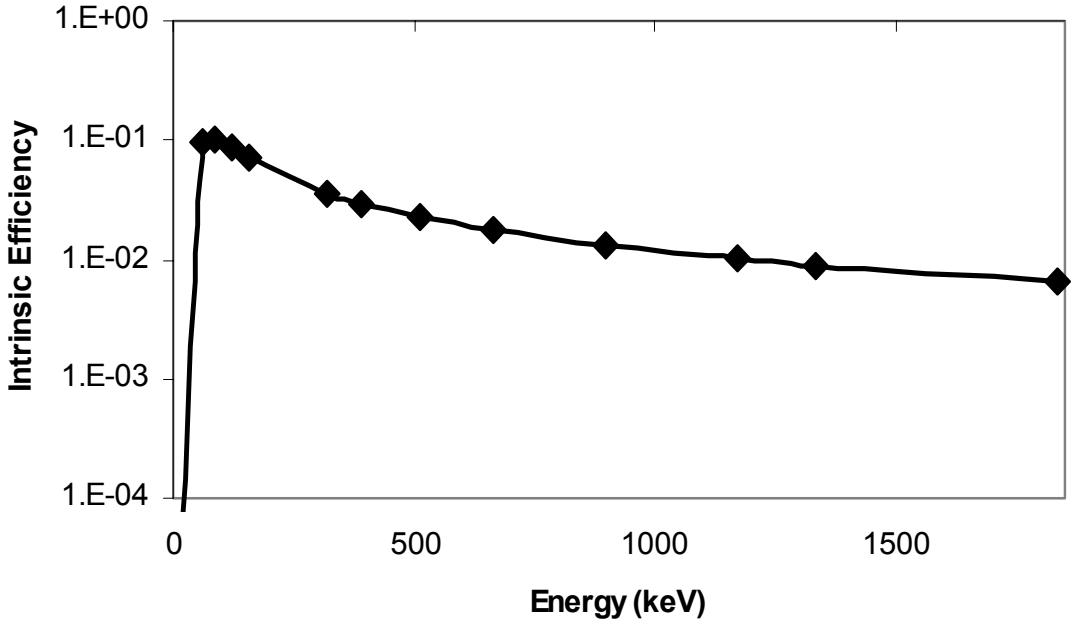

Figure 16 Intrinsic peak efficiency of the LN_2 HPGe detector as a function of incident gamma energy with the source located on the front of the face of the detector

Detector Resolution

Each detector's resolution (R) was then calculated using the formula below.

$$R = \frac{FWHM(keV)}{H_o(keV)} \tag{11}$$

where H_o is the energy of the peak channel. The results of resolution calculations are shown in Table 3. The FWHM of the EMC and LN_2 HPGe detectors, and the HgI_2 detectors at the region of interest (Cs-137 peak, 662 keV) was approximately 11.51 keV, 1.69 keV, and 22.61 keV respectively.

Table 3 Resolution calculation results for the HgI_2 and HPGe detectors

	Key Gamma (keV)	FWHM (keV)	Resolution (FWHM/ Key Gamma)
HgI_2 Detector	59.5	5.41	0.0909
	88.0	6.09	0.0692
	122.1	7.74	0.0634
	159.0	7.80	0.0491
	320.1	16.50	0.0515
	391.7	11.98	0.0306
	514.0	20.88	0.0406
	661.6	22.61	0.0342
	898.0	25.33	0.0282
	1173.2	14.38	0.0123
	1332.5	37.65	0.0283
EMC HPGe Detector	320.1	11.352	0.0354
	391.7	11.505	0.0294
	514.0	11.965	0.0233
	661.6	11.505	0.0174
	898.0	12.272	0.0137
	1173.2	11.505	0.00981
	1332.5	11.505	0.00863
LN_2 HPGe Detector	59.5	1.15	0.0193
	88.0	1.19	0.0135
	122.1	1.22	0.00999
	159.0	1.26	0.00792
	320.1	1.40	0.00437
	391.7	1.47	0.00375
	514.0	1.57	0.00305
	661.6	1.69	0.00255
	898.0	1.90	0.00212
	1173.2	2.13	0.00182
	1332.5	2.25	0.00169
	1836.0	2.64	0.00144

The resolutions for the HgI_2 detector illustrated the difficulty encountered in establishing the proper peak area for calculating the values shown. The first several peaks' efficiency proved to be reliable, but energies above 400 keV had errors in the peak area of over 20 percent, primarily because of hole-tailing effects and Compton scatter associated with the small size of the detector.

Subsequently, the FWHM calculations were very questionable. FWHM calculations were performed in the same manner as the manufacturer of the detector calculated FWHM, in order to make direct comparisons of resolution. The asymmetric full energy peak and critical points are displayed in Figure 17 riding on top of a continuum. The somewhat arbitrary nature of establishing the low end of the peak made the change of just a few counts alter the FWHM reading from a few keV to an infinite value as the low energy end never dropped much beyond the FWHM level.

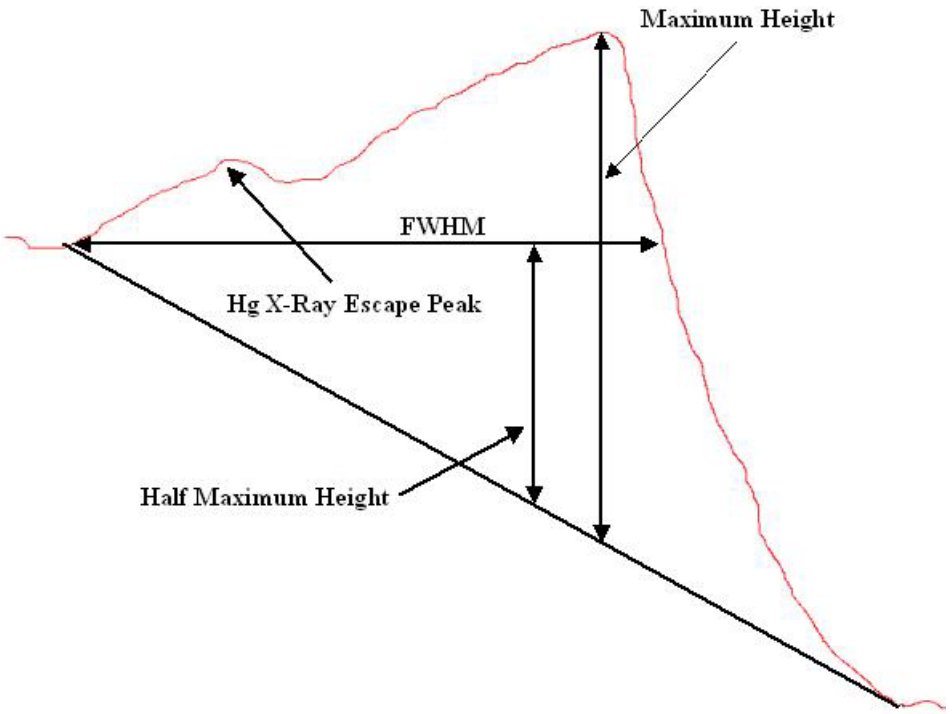

Figure 17 Key locations for calculating FWHM of an asymmetric HgI_2 peak owing to hole-tailing and Compton scatter effects riding on a Compton background

Detector Efficiency

Each of the detectors collected spectra with a different geometry. Refer to Appendix E for the methods used to make the solid angle approximation. The source was located 8 cm from the face of the HgI_2 detector. The crystal was located 5 mm below the surface of the detector for a total

distance of 85 mm. The source radius was 2.5 mm and detector area was 10 mm x 10 mm. Since the detector is not circular, an approximation was made using a circular detector of 100 mm^2. The radius using this approximation is 5.64 mm. The solid angle subtended by the HgI_2 detector was 1.56 x 10^{-2} steradians. The source was placed 30 cm in front of the EMC HPGe detector. The total distance between the detector and the source was 30.5 cm owing to an additional 5 mm from the surface of the detector to the crystal. The source diameter remained the same, but the crystal radius was 35 mm. The solid angle subtended by the EMC HPGe detector was 4.27 x 10^{-2} steradians. The multinuclide source was placed directly on the face of the LN_2 HPGe detector. Because the crystal was located 5 mm below the surface of the detector, the distance between the source and the detector was 5 mm. The solid angle subtended by the LN_2 HPGe detector was 5.08 steradians.

Given the information above, the detector's intrinsic peak efficiency (ε_{ip}) can be calculated from the following equation (16:118)

$$\varepsilon_{ip} = Cp/(\frac{\Omega}{4\pi} * S)\,. \tag{12}$$

The solid angle, Ω, is in steradians, *Cp* is the number of counts under the photopeak, and *S* is the number of decays per gamma energy. Comparisons using the intrinsic efficiency give a better comparison of the detectors, even though the measurements are still dependent on the geometry used in the individual experiment. Table 4 shows the intrinsic peak efficiencies for each of the detectors. The EMC HPGe could not be evaluated at the lower energy levels because of noise within the detection system.

Table 4 Intrinsic peak efficiencies of the HgI_2 ($\Omega/4\pi = 0.00124$), EMC HPGe ($\Omega/4\pi = 0.00340$), and LN_2 HPGe ($\Omega/4\pi = 0.404$) detectors with the photopeak counts normalized to one hour

	Key Gammas (keV)	Gammas Recorded, Cp (counts/hr)	Gammas Emitted by the Source, S (counts/hr)	Intrinsic Peak Efficiency
HgI_2 Detector	59.5	7939	7.30E+06	8.77E-01
	88	5254	6.37E+06	6.65E-01
	122.1	3403	5.60E+06	4.90E-01
	159	1812	5.91E+06	2.47E-01
	320.1	574	8.67E+06	5.34E-02
	391.7	576	1.71E+07	2.72E-02
	514	398	2.97E+07	1.08E-02
	661.6	646	2.68E+07	1.94E-02
	898	589	4.86E+07	9.77E-03
	1173.2	346	3.73E+07	7.48E-03
	1332.5	179	3.73E+07	3.87E-03
EMC HPGe Detector	320.1	12950	1.11E+07	3.43E-01
	391.7	17825	1.81E+07	2.90E-01
	514	27615	3.30E+07	2.46E-01
	661.6	18185	2.68E+07	2.00E-01
	898	29513	5.19E+07	1.67E-01
	1173.2	17407	3.73E+07	1.37E-01
	1332.5	16570	3.74E+07	1.30E-01
LN_2 HPGe Detector	59.5	687500	7.29E+06	2.33E-01
	88	612500	6.21E+06	2.44E-01
	122.1	454167	5.33E+06	2.11E-01
	159	375833	5.50E+06	1.69 E-01
	320.1	195000	5.50E+06	8.77E-02
	391.7	450000	1.53E+07	7.28E-02
	514	529167	2.45E+07	5.35E-02
	661.6	466667	2.67E+07	4.33E-02
	898	520833	4.33E+07	2.98E-02
	1173.2	362917	3.70E+07	2.43E-02
	1332.5	317083	3.70E+07	2.12E-02
	1836	281667	4.58E+07	1.52E-02

Figure 18 displays plots of the intrinsic peak efficiencies calculated in Table 4. Examination of the plots reveal that the shape of the curves are as expected for the 300 keV to 1300 keV portion of the spectra. The efficiency of the LN_2 HPGe detector reflects a lower efficiency than the EMC

HPGe detector because of the 5 mm separation distance between the source and the detector. The short distance made it possible for gammas to pass through the sides of the detector (up to one mean free path) without interaction. This loss, of gamma interactions, lead to an apparent loss in efficiency. Some variation exists in the slope of the HgI_2 curve near the 662 keV peak because of the errors associated with the calculation of the peak area. A better comparison could have been made if the geometries had been similar.

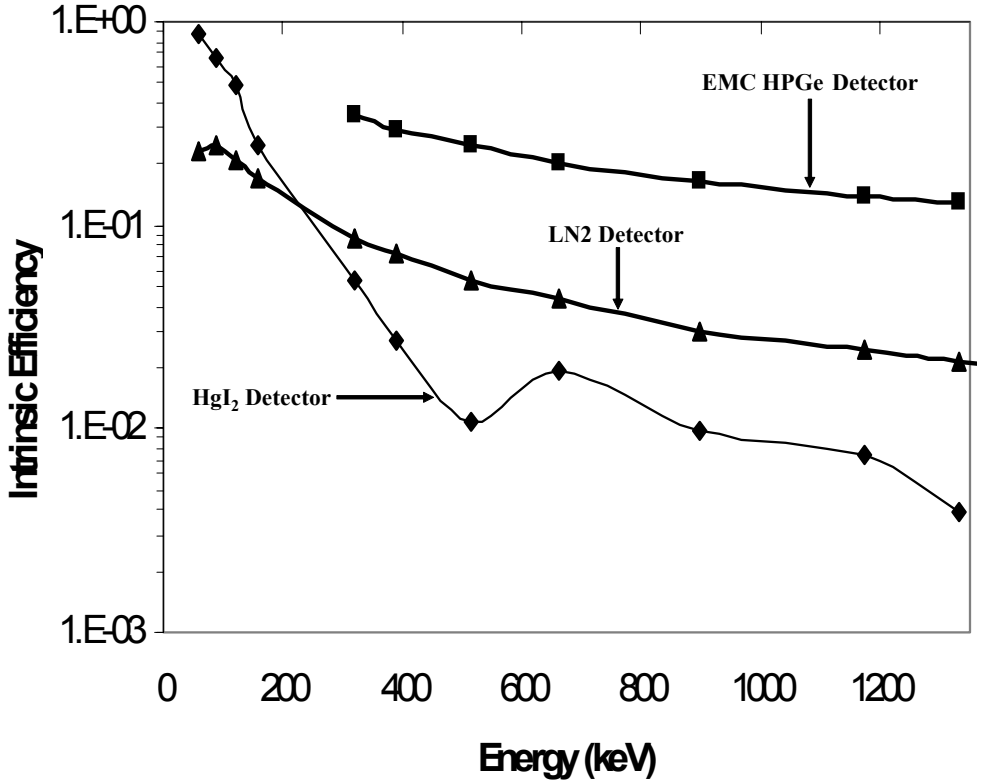

Figure 18 Intrinsic peak efficiencies of the HgI_2 and HPGe detectors using solid-angle approximations

Detector Comparison

Comparison of Uranium Spectra

Figure 19 shows the background stripped spectrum gathered by both the HgI_2 and EMC HPGe detectors from a natural uranium ore. The source was placed 30 cm in front of the EMC HPGe detector for a ten-hour (live time) spectral data collection time. The source was placed 8 cm in front of the HgI_2 detector for a twelve-hour (live time) spectral data collection time. The information obtained by each of the detectors is sufficient to determine that the test sample is a natural uranium ore due the decay daughters of U-238 (Bi-214 and Pb-214) and U-235 (Bi-211 and Pb-211).

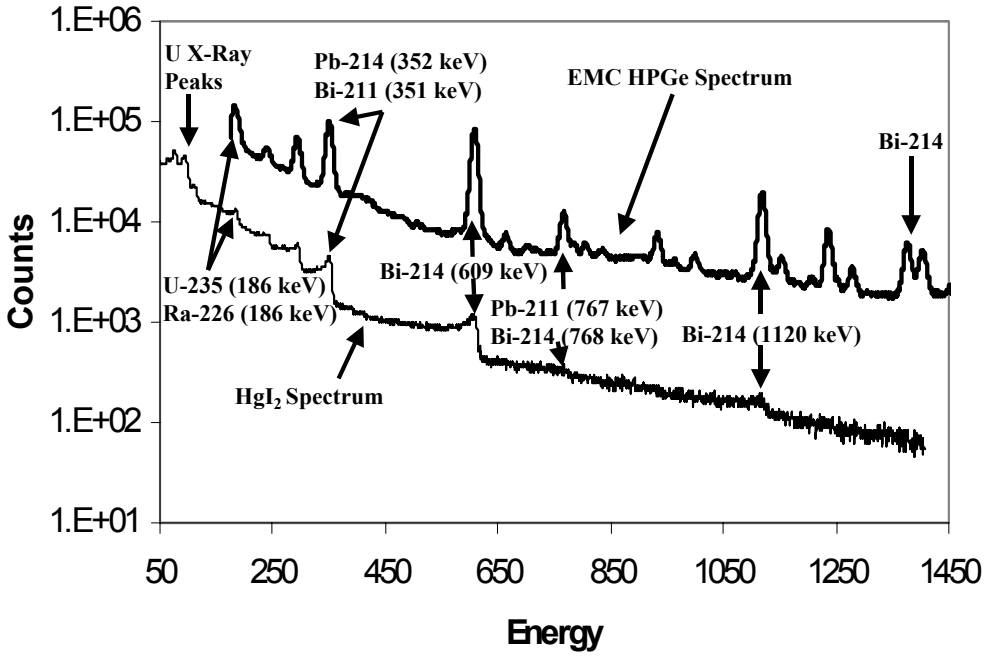

Figure 19 Natural uranium ore spectra comparison of a 10-hour (live time) EMC HPGe spectrum and a 12-hour (live time) HgI_2 spectrum. The source was placed 8 cm in front of the HgI_2 detector and 30 cm in front of the EMC HPGe detector.

The prominence of several Bi-214 in both spectra clearly demonstrated the overall abundance of the U-238 decay chain. The daughter elements that complicated the spectra are not present in

weapon-grade uranium (12:266). The most prominent gamma peak (186 keV) for U-235 released is the same energy level as one of the U-238 decay chain daughters (Ra-226), making identifying the isotopic mass ratio or the two uranium isotopes more complex. The electronics' lower level discriminator eliminated the most prominent gamma peaks for U-235 (19.59 keV) to reduce dead time in the 640 keV range.

The most complex issue for identification remains the lack of penetrating gammas released by either isotope of uranium. Appendix A shows that U-235 had only three gammas likely to escape the shielding of a SNM container: a 202 keV, a 205 keV, and a 221 keV gamma. U-238 had no prominent gammas likely to escape the shielding of a SNM container because they all have energies less than 200 keV. These conditions make the identification of weapons grade uranium a very complex problem.

Comparison of Plutonium Spectra

Figure 20 shows the spectra gathered by both the HgI_2 and the EMC HPGe detectors from a plutonium source. A twelve-hour spectrum (live time) for the HgI_2 detector, and a ten-hour spectrum (live time) for the EMC HPGe detector was collected using the same geometry as specified for the detector calibrations. From the information obtained from each of the detectors it was determined that the test sample contained both Pu-239 and Am-241, but there was insufficient data to determine the plutonium grade of the sample. Appendix H shows the isotropic make up of the plutonium sample used throughout the project to be approximately 80 percent Pu-239 to 20 percent Pu-240.

The americium and plutonium were easily seen by the presence of several large, key Am-241 gamma peaks and the smaller Pu-239 peaks at the lower energy levels. Since there was no

information on whether there was any Am-241 in the original sample, it could not be determined whether the existence of Am-241 was primarily the result of beta decay from Pu-241 or if large quantities were in the test sample originally. It is probable that Am-241 existed in the sample at the time of acquisition since the sample would qualify as fuel grade plutonium.

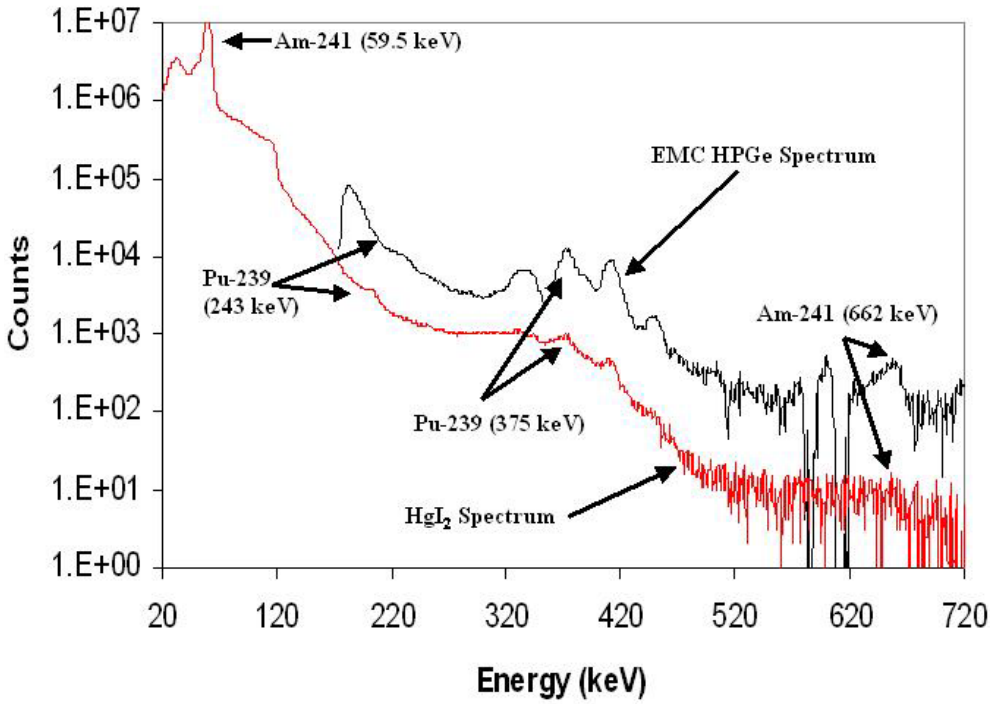

Figure 20 Plutonium spectra comparison of a 10-hour EMC HPGe spectrum and a 12-hour HgI_2 spectrum

Figure 21 shows an enlargement of the 640 keV range of interest for determining isotopic concentrations for plutonium. The results shown in the enlargement bring both detectors' ability to determine the grade of plutonium into question unless the SNR is improved. Capabilities became questionable after a minimum of ten hours spent collecting spectra. It is improbable that sufficient counts could even be obtained within the time constraints allowed as an inspector attempts to collect spectral information.

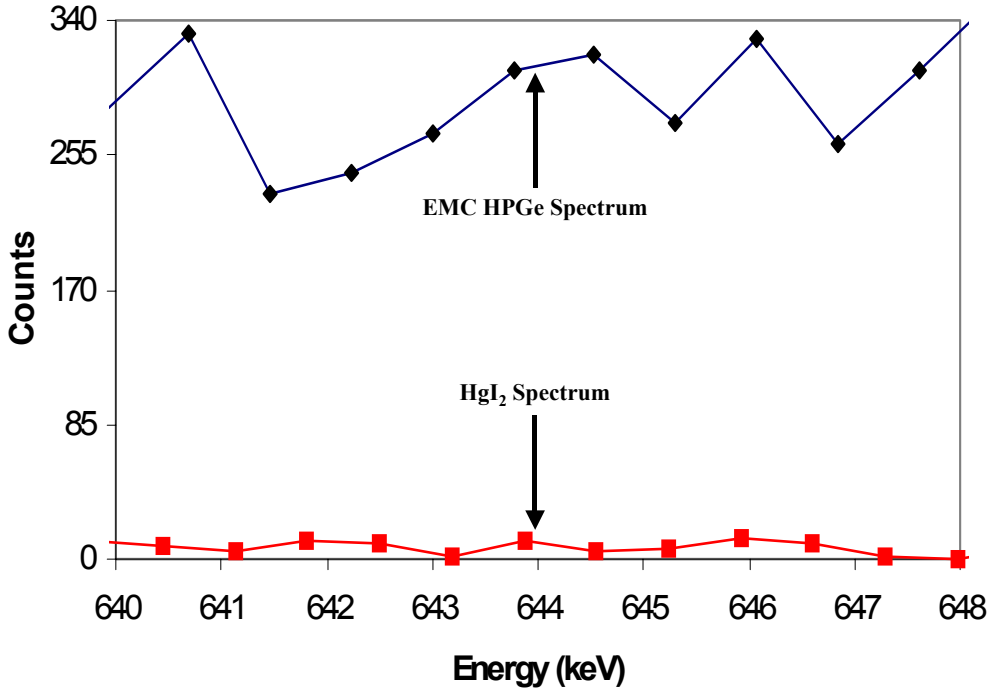

Figure 21 Expanded plutonium spectra of a 10-hour (live time) EMC HPGe spectrum collected from 30 cm and a 12-hour (live time) HgI_2 spectrum collected from 8 cm

Simulated and Derivative SNM Spectra

The procedures used to obtain both the simulated and derivative spectra are found in Appendix H as shown for the evaluation of the LN_2 HPGe detector.

Comparison of Simulated Plutonium Spectra

Figure 22 shows results obtained from simulated EMC HPGe detector spectrum and Figure 23 shows results obtained from simulated HgI_2 detector spectrum. These results demonstrated that neither of the detectors could resolve the Pu-239 and Pu-240 peaks to allow for the determination of the grade of plutonium without improvement to the detectors' response function. Figure 24 shows the simulated spectrum obtained from the LN_2 HPGe detector for comparison purposes.

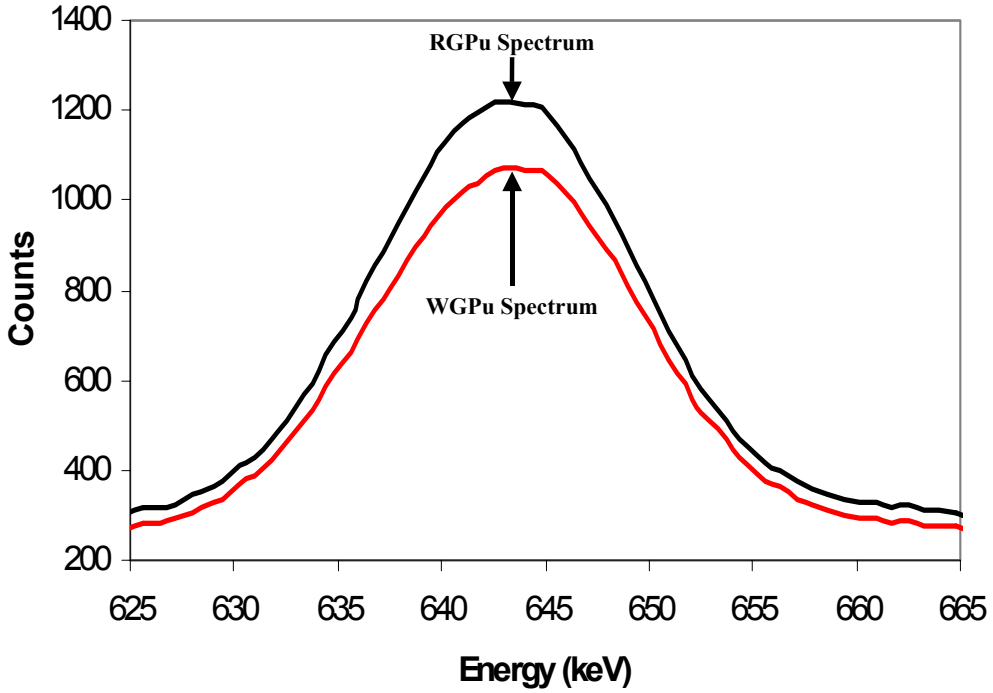

Figure 22 Simulated plutonium spectra comparing the WGPu and RGPu for the EMC HPGe detector

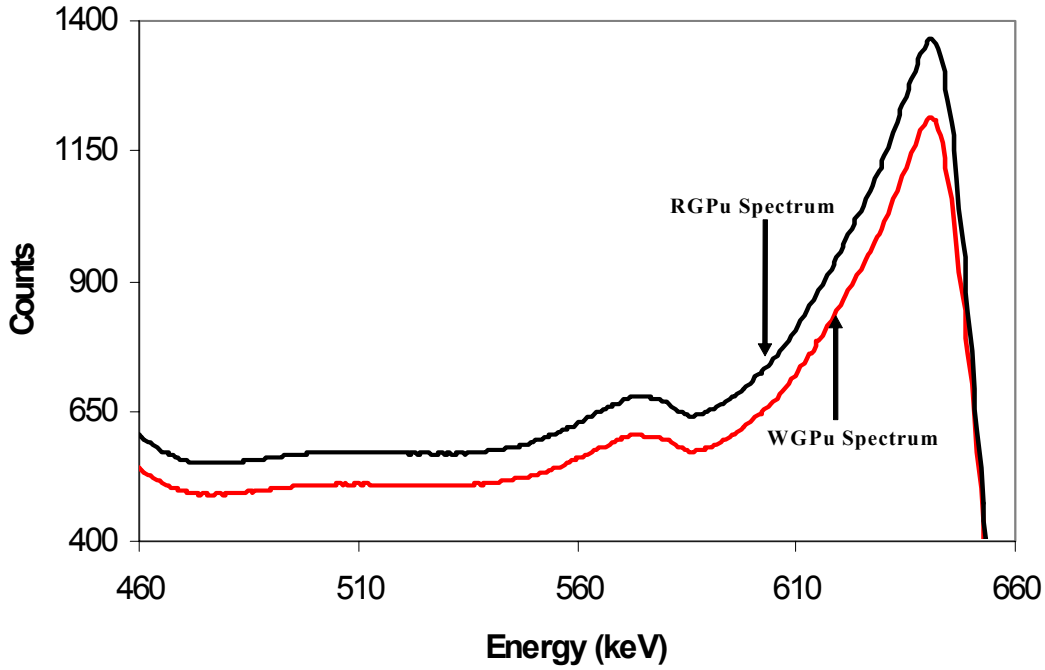

Figure 23 Simulated plutonium spectra comparing WGPu and RGPu for the HgI_2 detector

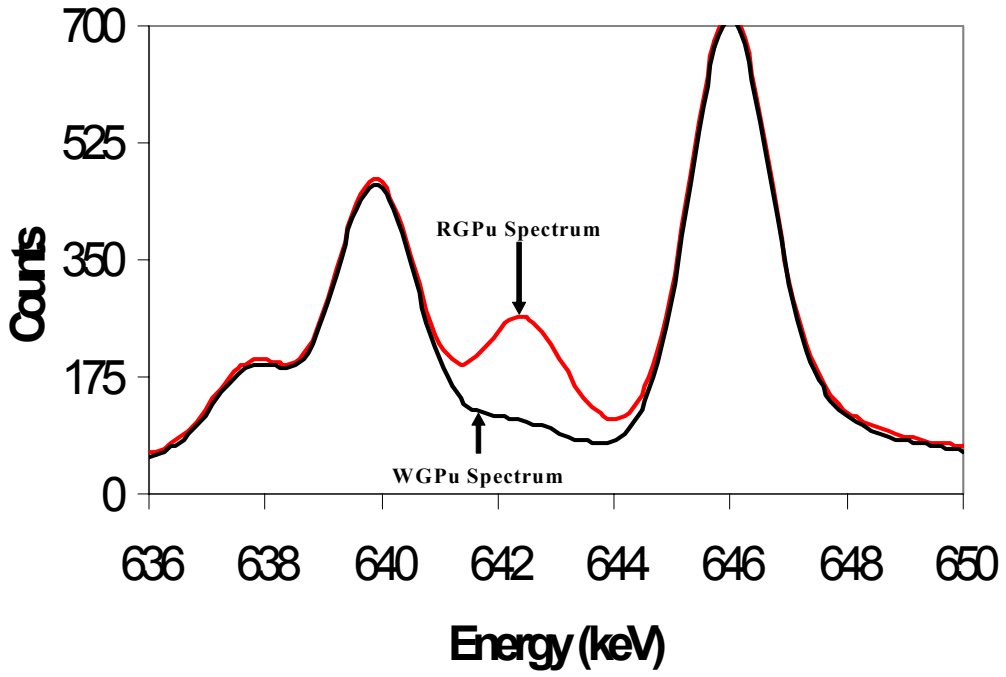

Figure 24 Simulated plutonium spectra comparing WGPu and RGPu for the LN_2 HPGe detector

Both the HgI_2 spectra and the EMC HPGe spectra contained a single peak in the 640 keV region, the convoluted collection of Pu-239, Pu-240, and Am-241 peaks. The smaller peak in the HgI_2 spectra can be easily identified as an Hg X-ray escape peak associated with the HgI_2 detector. The simulated LN_2 HPGe displays clear evidence of deconvolved peaks. This resolution demonstrates the level type of results being sought from the experimental detectors. A good deconvolution program may be capable of pulling the information from the single peak in the HgI_2 and EMC HPGe spectra. In order to get the information from the convoluted spectra, the derivatives of the spectra were examined for changes in the slope where the energy peaks overlap.

Comparison of Derivative Plutonium Spectra

Figure 25 shows the derivative of a simulated EMC HPGe detector spectrum, Figure 26 shows the derivative of simulated HgI_2 detector spectra, and Figure 28 shows the derivative of the LN_2

spectra for comparison purposes. The ragged appearance of the derivative spectra demonstrates the high noise apparent in both spectra.

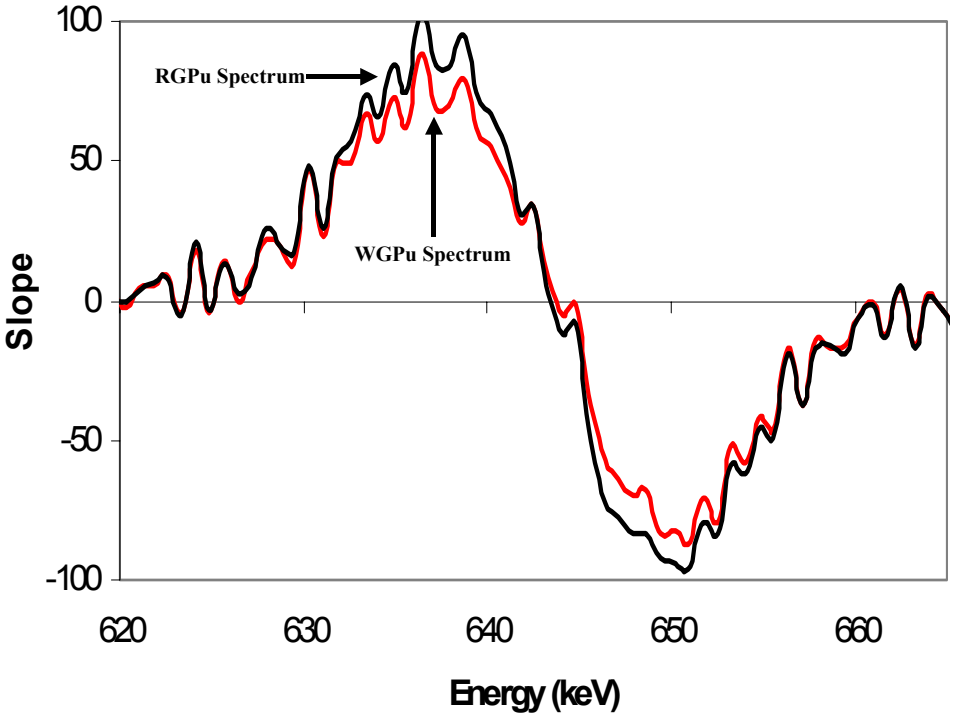

Figure 25 Derivative of simulated plutonium spectra comparing the WGPU and RGPu for the EMC HPGe detector

Both spectra cross the zero axis around 642 keV. This demonstrates that only one peak exists within the EMC HPGe spectra for either grade of plutonium. Because of the high level of noise visible in the derivative, a second derivative was not taken.

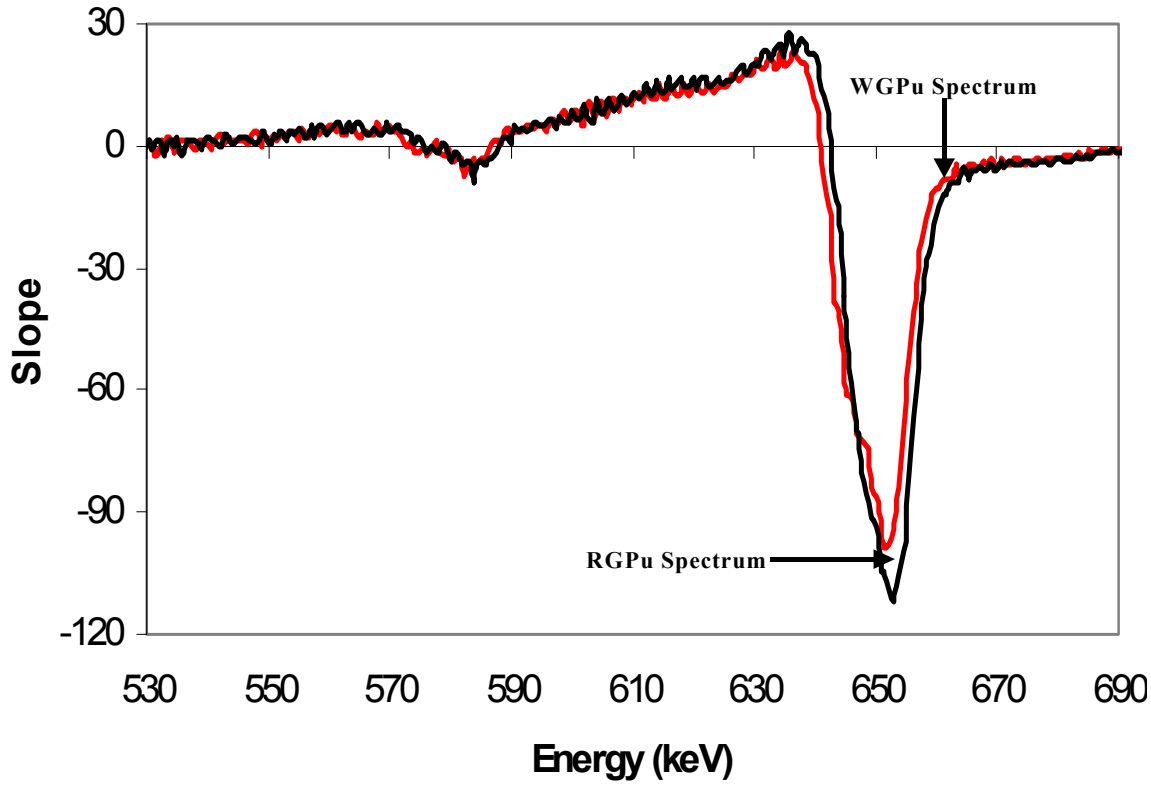

Figure 26 Derivative of simulated plutonium spectra comparing the WGPu and RGPu for the HgI_2 detector

The HgI_2 derivative spectra show the only peaks in the spectra are the result of the convoluted peak around 640 keV and the Hg escape peak at approximately 580 keV. The derivatives cross at approximately 645 keV, which could be an indication of the different plutonium and americium peaks. In order to investigate the cause of this feature, a second derivative was taken and the results are shown in Figure 27.

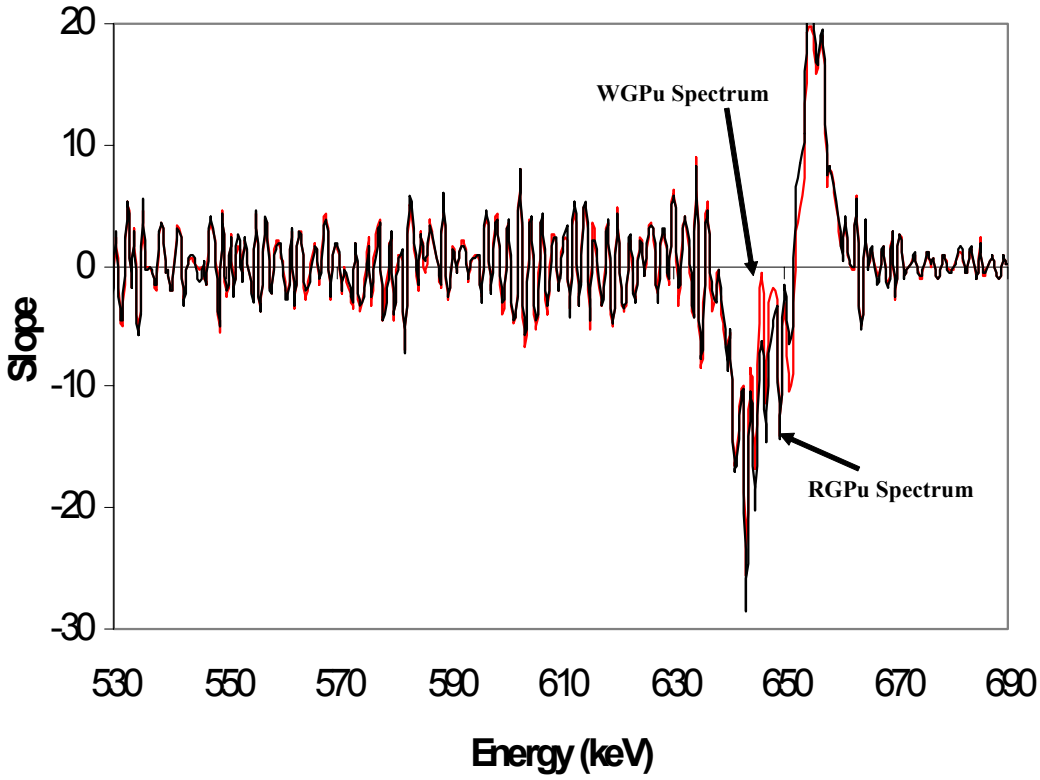

Figure 27 Second derivative of simulated plutonium spectra comparing the WGPu and RGPu for the HgI_2 detector

Examination of the second derivative of the HgI_2 spectrum reveals that the crossover in the first derivative was the result of the iodide escape peak. This shows that more information about the nature of the spectra can be determined from additional derivatives. Because of the level of the noise in the second derivative, a third derivative did not reveal new information about the make-up of the convoluted peaks.

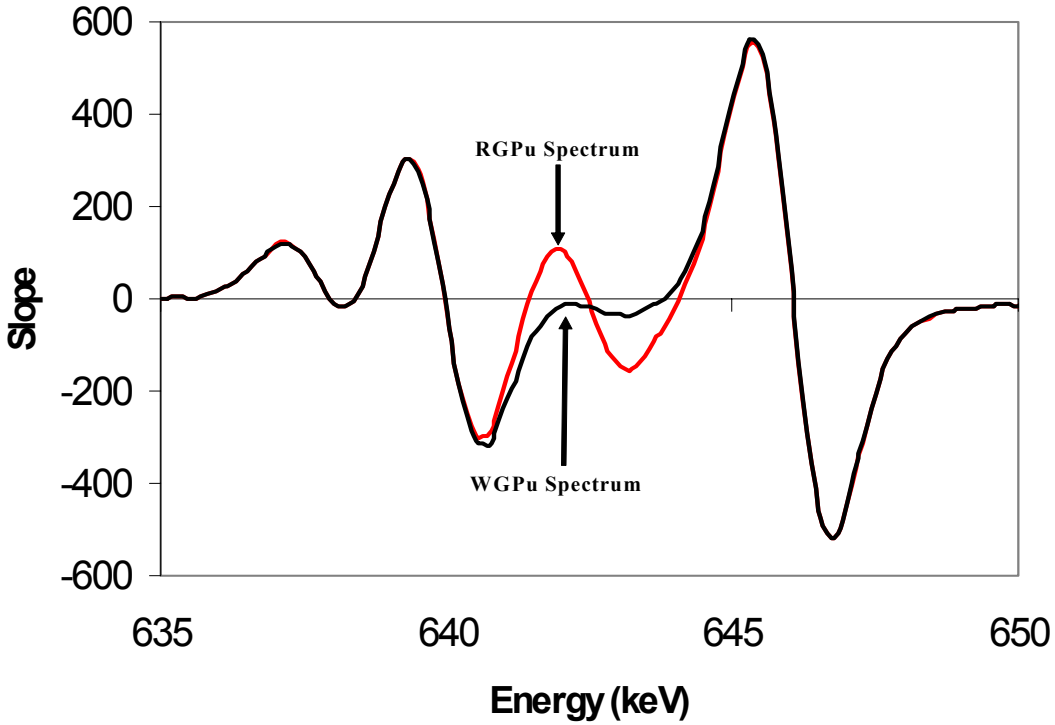

Figure 28 Derivative of simulated plutonium spectra comparing the WGPu and RGPu for the LN_2 HPGe detector

Unlike the results obtained with the experimental detectors, each of the plutonium peaks can be identified in the derivative. The change in slope for WGPu for the Pu-240 energy peak vice the clear peak for the Pu-240 energy peak for the RGPu shows the manner in which the derivative spectra can differentiate between the two grades of plutonium. The second derivative of the LN_2 HPGe spectra is shown in Figure 29.

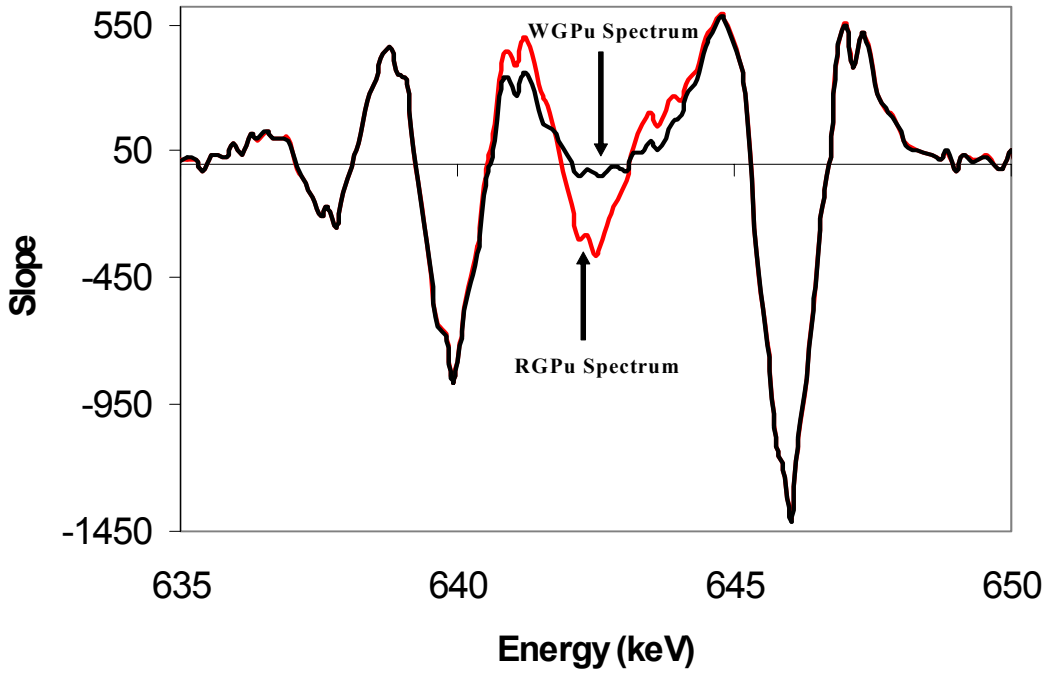

Figure 29 Second derivative of simulated plutonium spectra comparing the WGPu and RGPu for the LN_2 HPGe detector

Examination of the second derivative of the LN_2 HPGe spectra reveals differences in the spectra at approximately 642 keV. It cannot be conclusively determined whether the differences at 642 keV are the result of the Am-241 peak or the noise becoming apparent within the spectra.

EMC HPGe Power Level Analysis

The EMC HPGe detector offers three cooling power settings for collecting spectra. The normal cooling mode maintains regulating temperature for constant operations. The low power option maintains cooling at approximately half that of the normal power operations. While this option allows for a proportional reduction in the low frequency vibrational noise associated with the cryocooler, the temperature of the crystal warms slowly. The detector also offers the option to collect spectral data with the cryocooler turned off for a short time. This condition allows for an additional reduction in noise, but the crystal warms faster.

Two experiments were conducted to examine the results obtained by using the different power settings. The first experiment was used to examine the number of containers that could be measured before the detector cycled from regulating mode to cooling mode. One minute elapsed between trials (with the detector in regulating mode) to simulate moving the detector from one container to another container to collect a spectrum. Typical results obtained from each power mode are shown in Table 5. After cycling into cooling mode, the EMC HPGe detector took approximately one-hour to cool enough that it could operate in the normal regulating mode.

Table 5 Number of trials before the EMC HPGe detector cycled into cooling mode from operating mode under different power conditions

Spectra Acquisition Time (min)	Low Power		No Power	
	# Trials	Average Rise in Temp / Trial (K)	# Trials	Average Rise in Temp / Trial (K)
2	5	1	3	2.33
5	3	2.67	2	5.50
15	1	7	1	12

The second experiment was used to examine the change in resolution resulting from the change in power settings. The degradation became clear when comparisons of the FWHM and Full Width-Tenth Maximum (FWTM) were calculated. FWHM and FWTM for each of the three power settings are shown in

Table 6.

In addition to the changes in resolution and peak channel counts, the energy calibration also appeared to be affected by the power setting. As the peak count rose with the lower power setting, the location of the peak channel shifted down in energy an average of 0.5 keV. The implications of this are beyond the scope of this project.

Table 6 FWHM, FWTM, and peak count comparisons for the three possible power conditions of the EMC HPGe detector

	FWHM	FWTM	Peak Counts
Normal Power	11.437	21.109	384
Low Power	9.979	14.891	429
No Power	9.595	14.508	456

The lower power levels give clear evidence of the benefits of the detector in a lower power setting. Additional experiments are required to verify the benefits when the resolution is improved. The actual decision to use the lower power settings will depend on the number of SNM containers to be evaluated.

EMC HPGe Grounding Loop Problem

A major problem identified with the EMC HPGe detector was with the grounding loop that affected the resolution. Figure 30 shows the effect of the error for a spectrum from a Cs-137 source. The electronics remained plugged into the AC outlet for the first experiment. The electronic settings remained the same as the first experiment, except that the transport case was unplugged from the wall. In both experiments, the gamma spectrum was collected while operating the cryocooler off of the battery power stored in the transport case. Table 7 displays the changes in the resolution and the peak counts upon unplugging the electronics from the AC power source.

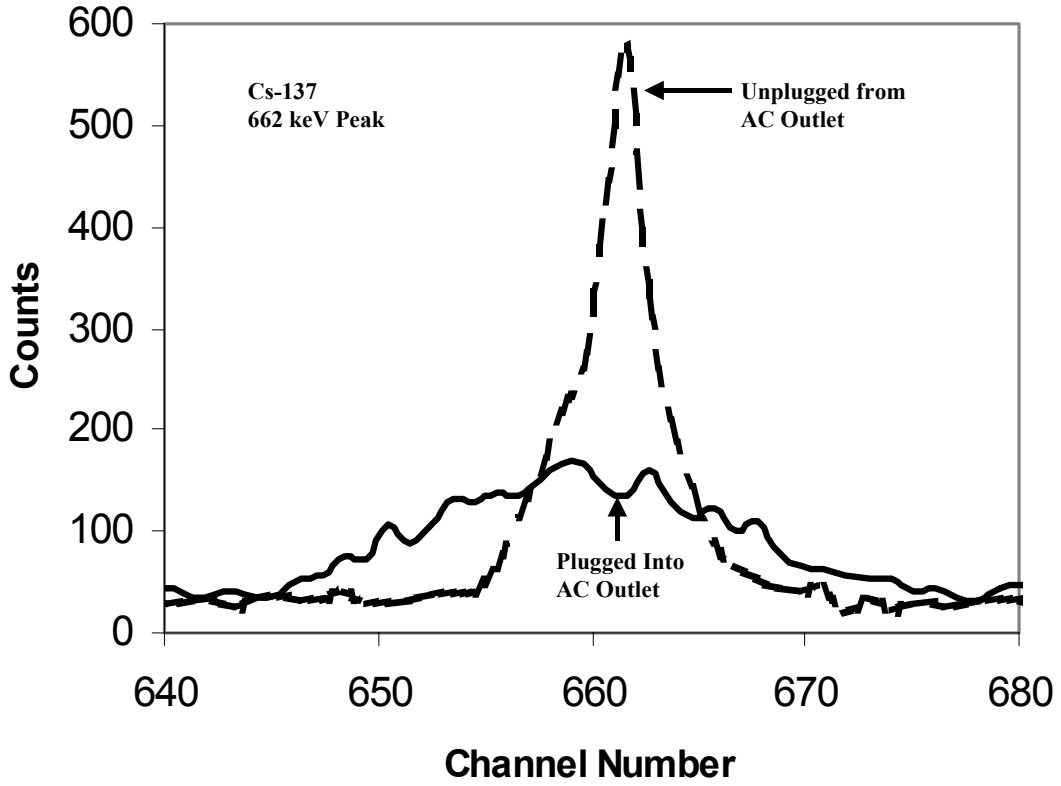

Figure 30 662 keV photopeak spectra comparison of ground loop problem using a Cs-137 point source

Table 7 FWHM, FWTM, and peak count comparisons for ground loop problem for the EMC HPGe detector

	FWHM (keV)	FWTM (keV)	Peak Counts
System Plugged In	16.368	28.542	579
System Unplugged	3.069	10.025	168

The results obtained with the system unplugged from the AC power source still need to be improved as the FWTM is still greater than twice the FWHM (16:435). The grounding loop data resulted from a single experiment as the detector experienced other problems after discovering the grounding error.

Weapon Mock-Up Characterization

The LN_2 HPGe detector was used to collect all the spectra from the different mock-up configurations. The bowl source was located at a distance of approximately 38 cm on axis with the front face of the detector. The simulated reflector and tamper were placed into position without changing the location of the bowl source. Figure 31 shows an enlargement of the gamma spectra gathered from different configurations of the mock-up, normalized to the Cs-137 full energy peak. The peaks where normalized by scaling the magnitude of the different mock-up configurations, so that the full energy peak channel contained an identical number of counts for all three configurations. No other magnitude scaling was performed on the peaks. No energy scaling was performed as all the spectra were collected under the same energy calibration. The exposed sides of the LN_2 HPGe detector were shielded by a minimum of five centimeters of lead to reduce the amount of Compton scatter from the source coming into the detector from off the walls of the tomb.

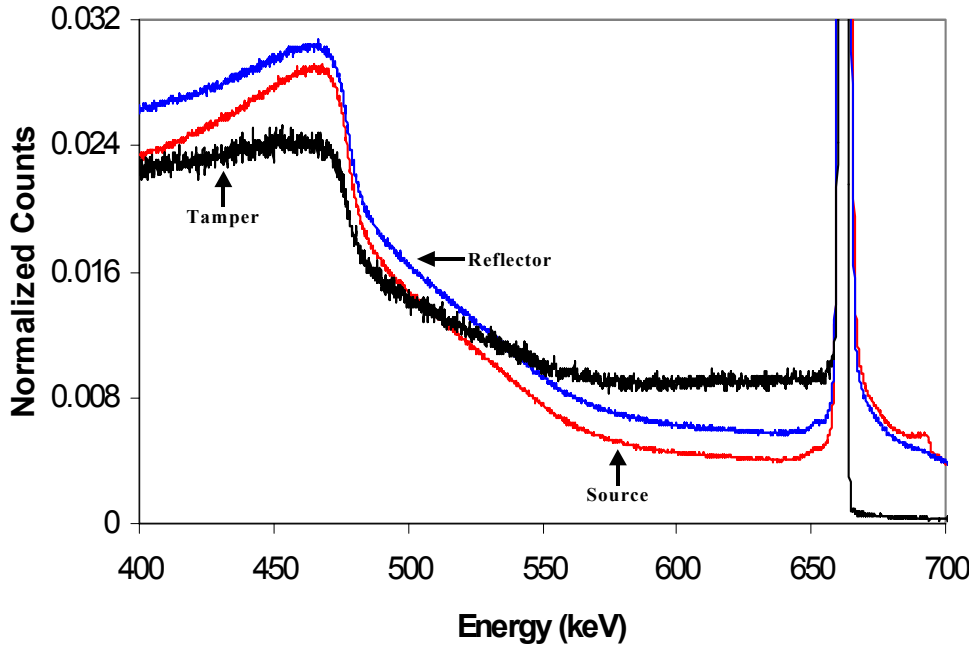

Figure 31 Comparison of normalized mock-up LN_2 HPGe spectra consisting of source, reflector, and tamper spectra collected from approximately 38 cm

Table 8 displays the gamma energy and count information obtained from the spectral information with the mock-up in the configurations shown above. The information from the point source is included for comparison purposes.

Table 8 Channel locations of key features collected from mock-up counting experiments and the total number of gamma counts obtained in key locations

Configuration	Peak Energy (keV)	Valley Energy (keV)	Leading Edge Energy (keV)	Peak Counts	Valley Counts	Leading Edge Counts
Point Source	661.7	604.4	461.9	34193	34	547
Source	661.7	638.3	467.7	1744316	6879	3301
Reflector	661.7	639.1	466.6	1407095	7879	3293
Tamper	661.7	574.7	452.7	126181	1047	3195

Table 9 displays key gamma count ratios obtained with the mock-up. These are ratios of the counts in the peak channel to the counts in each of the remaining key channel locations.

Table 9 Comparison of key gamma count ratios for different mock-up conditions ratios

	Point Source	Bowl Source	Source and Reflector	Source, Reflector, and Tamper
Peak-to-valley Ratio	1005.7	253.6	178.6	120.5
Peak to Leading Compton Edge Ratio	62.5	34.2	32.5	39.5

Figure 32 through Figure 36 show enlargements of the peak-to-valley ratio, small peak location, peak-to-Compton leading edge ratio, and the change in the location of the knee leading from the peak to the Compton leading edge.

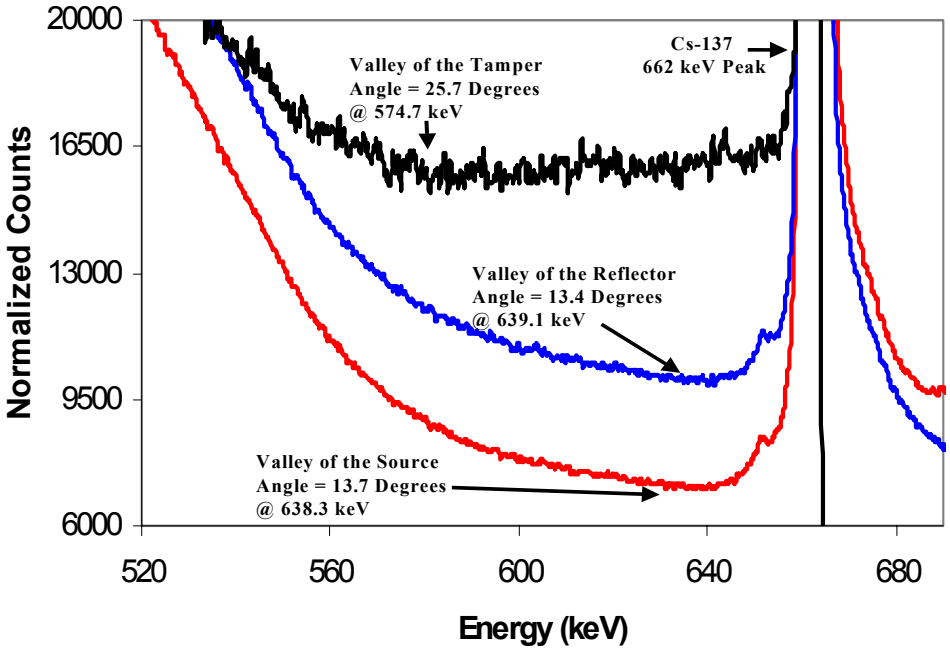

Figure 32 Normalized spectra with the location of the valley used in the peak-to-valley ratio marked

The valley is the primary feature displayed in the 570 keV to 640 keV range. The peak-to-valley ratio decreases from 253.6:1 to 178.6:1 with the addition of the reflector because of photoelectric absorption. There is a 0.3 degree change to the location of the valley from Compton effects. The addition of the tamper caused a decrease in the peak-to-valley ratio to 120.5:1. The Z value of the tamper is much higher than the air and caused the Compton scatter angle associated with the tamper to increase by over 12 degrees.

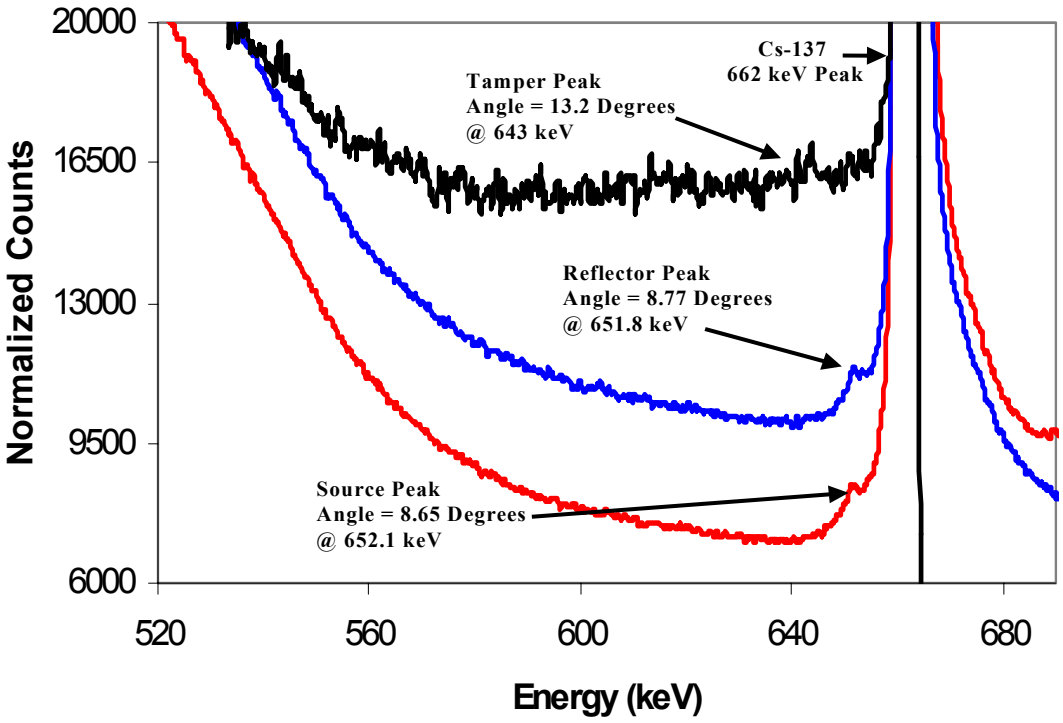

Figure 33 Normalized spectra with the location of a small Compton scatter peak marked

The small energy peak in the 640 keV to 655 keV energy peak was the result of a preferential Compton scatter angle associated with the geometry of the mock-up. The geometry of the bowl source is shown in Figure 34. The angle (α) indicates the maximum angle of scatter from within the bowl source to the detector. Under these conditions, the angle of scatter is approximately 7.5 degrees. The measured angle and the calculated angle differ by just over 1.2 degrees. This difference is because the bowl source is at an angle to the front face of the detector instead of parallel. The addition of the reflector and the tamper do not affect the geometry between the source and the detector. Adding the reflector had almost no change as would be expected. The additional Compton scatter caused by the tamper shifts the peak down by just over 10 keV and would be expected to broaden the energy peak. Although the energy peak appeared to behave as expected, the fluctuations in the tamper spectrum make the changes difficult to confirm.

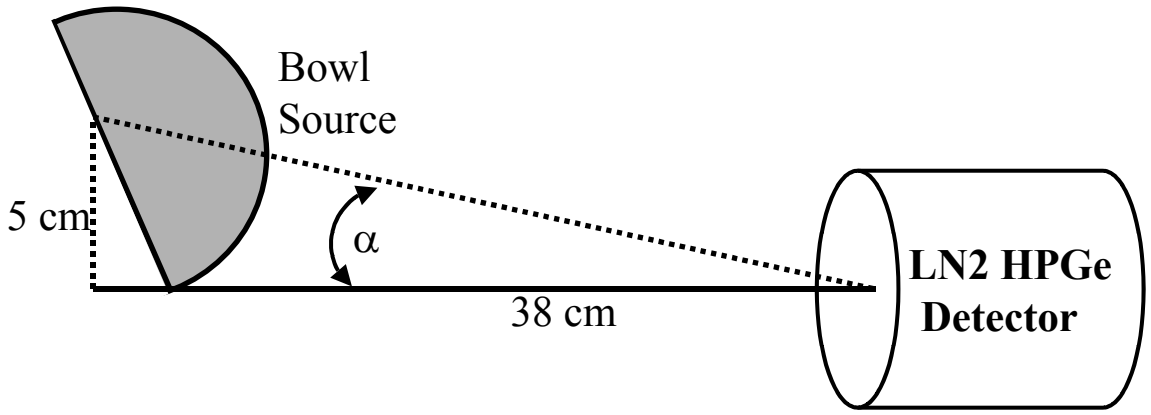

Figure 34 Side view of the geometry with the bowl source and the LN_2 HPGe detector

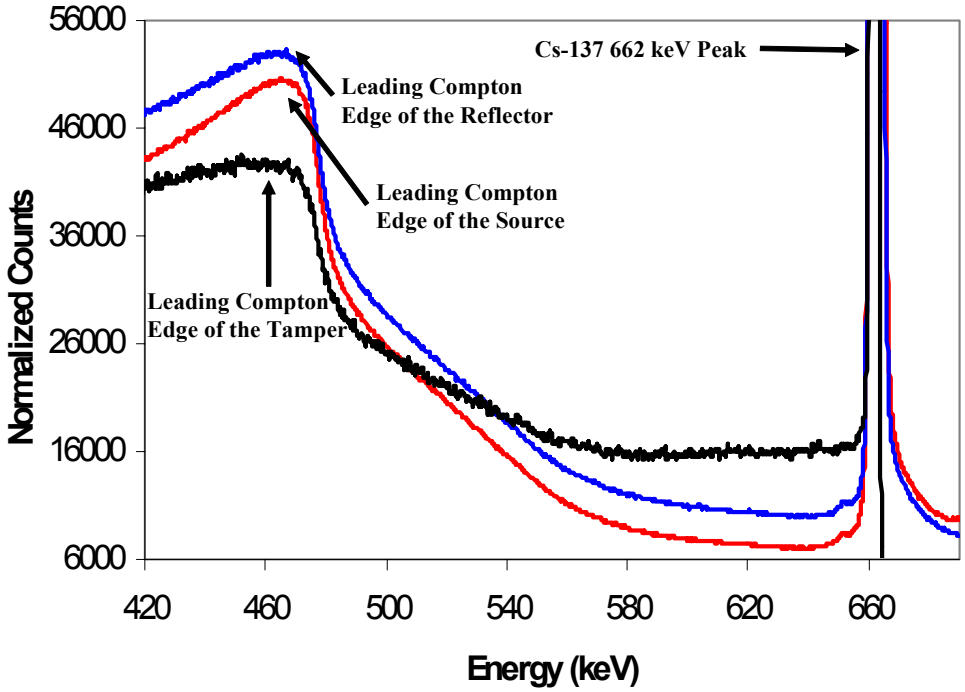

Figure 35 Normalized spectra with the location of the Compton leading edge used in the peak-to-valley ratio marked

The Peak to leading Compton edge ratio decreased with the addition of the reflector from 34.2:1 to 32.5:1 and increased with the addition of the tamper from 32.5:1 to 39.5:1. The decrease with the addition of the reflector resulted from the increased absorption material. The increase in the Peak to leading Compton edge, after the tamper was added, resulted from forward Compton scatter from the

Cs-137 peak into the 550 keV to 650 keV range. The increased counts in the 550 keV to 650 keV range meant fewer gammas available for backscatter events within the detector.

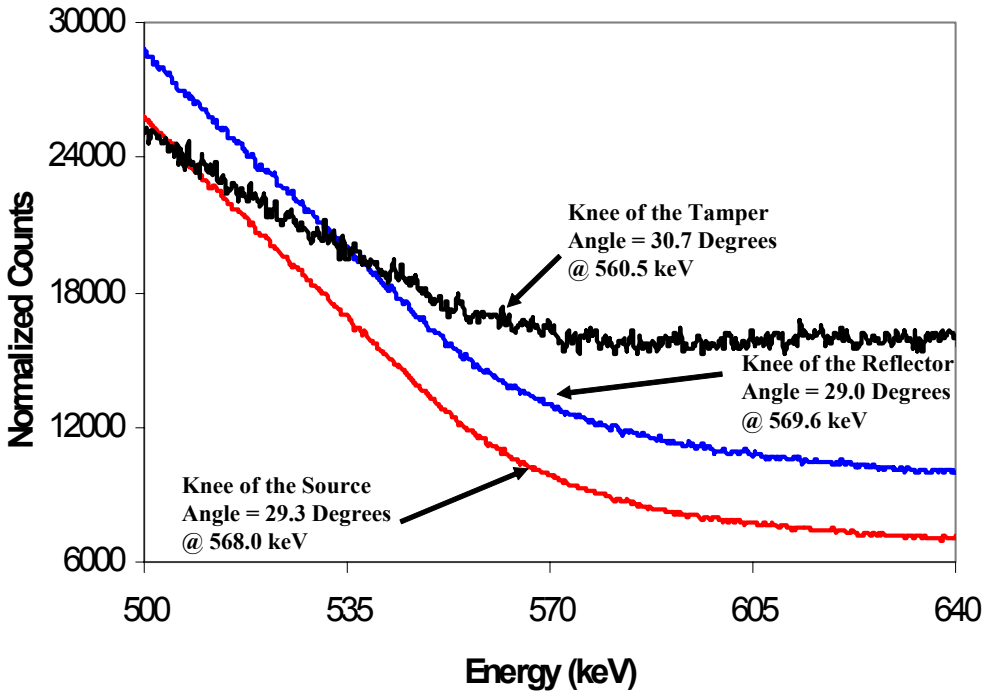

Figure 36 Normalized spectra with the location of the knee marked and the associated angle annotated

The knee formed by the multiple forward scatter events in the 600 keV to 640 keV range and the slope leading Compton edge changed significantly with the scatter material as compared to the absorbing material. Although the angle remained at approximately 145 degrees when the source and the reflector were in place, the angle increased by almost 10 degrees with the addition of the tamper. Additional scattering material eliminated this knee altogether, leaving a sharp increase in peak counts at the leading Compton edge.

V. Conclusions and Recommendations

Conclusions

The experimental detectors (HgI_2 and EMC HPGe) are not completely capable of performing the treaty verification mission set forth by DTRA. The HgI_2 detector evaluated cannot resolve the WGPu Pu-240 peak at 642.35 keV from the Pu-239 peak at 639.99 keV without improving the response function. The measured and modeled FWHM was greater than 20 keV at 662 keV vice the approximately 3 keV needed. The quality of the EMC HPGe spectra could not be resolved to the point of performing a proper analysis. Prior to the failure of the detector, the resolution at 662 keV was measured and modeled at 11.6 keV. For comparison purposes, the measured resolution of the LN_2 HPGe detector at 662 keV was 1.69 keV. Efforts to gain insight into the nature of the plutonium energy peaks included a simulated WGPu spectrum and a simulated RGPu spectrum along with each of their derivative spectra. Examinations of these spectra indicate that the intensities of WGPu and RGPu spectra are distinguishable at the lower resolution, but the mass isotope ratio of Pu-239 and Pu-240 could not be determined. This requires detectors with excellent efficiency or long count times. Distinguishing the grades of plutonium at a lower resolution requires some prior knowledge of the number of counts under the convoluted peak.

Experiments with spoof identification proved to be very promising. Clear evidence was documented that information such as a reduction in the peak-to-valley ratios under different physics package configurations could lead to the identification of a missing tamper, compensating for reduced plutonium. This might provide the ability to identify one method of spoofing a treaty verification team. Further study is needed to determine to the best approach to solving this problem.

Recommendations for Future Work

This research indicated several areas of future research. These included areas of detector research, improving the response function of HgI_2 detector and spoof identification research.

HgI_2/CZT Detector Research and Response Function Improvement

The HgI_2 detector offers great potential because of its smaller size, portability, and room temperature operation. Larger crystals available from Constellation would result in an increase of surface detection area by a factor of 6.25. This would allow for collimation experiments using Compton spectrometer configurations without decreasing the solid-angle subtended by the detector. CZT detectors have a similar response function to HgI_2 detectors The resolution obtained by prior CZT studies resulted in an approximately 15 keV improvement in the FWHM at 662 keV compared to the HgI_2 results obtained during this research (6:32).

Research in methods of improving the response function for detectors such as CZT and HgI_2 are recommended. One method is the use of a Compton spectrometer. Using the CZT detector or an HgI_2 as the first detector in the Compton Spectrometer and a high efficiency NaI(Tl) detector since coincidence checking is the key and resolution would not be important. This method should improve the detector response function without degrading the resolution by summing the area under the Compton distribution based upon the Compton scatter angle. Several experiments have already been conducted using Compton spectrometers to monitor SNM containers for SNM accountability purposes (2:867-9). Research into adapting this technology for treaty verification purposes warrants further research. A second method is Compton rejection by anticoincidence. The CZT detector or the HgI_2 detector could be placed in a Compton suppression system such as a NaI(Tl) and BGO well-type scintillator to reduce the Compton distribution spectrum. The primary advantage to both

of these systems is that the detectors used are relatively small, highly-mobile room temperature detectors.

EMC HPGe Detector Research

Alternate means of HPGe crystal cooling warrant additional research. The research attempted throughout this project with the EMC HPGe detector should be undertaken again if the grounding problem is resolved.

Better Spoof Identification

Several areas within spoof identification need additional research. They include researching improved mock-ups of a weapon physics package and a numerical model to predict the energy spectrum to be emitted by a distributed source. An in-depth study should be conducted on the features in the resulting spectra from the different conditions of a mock-up. In addition to more investigation into the peak-to-valley ratio and the peak to leading Compton edge ratio, better conditions need to be established to study the peak to backscatter ratio. Studies in an open environment similar to inspection conditions would tell the investigator what information might be drawn from this feature. Some of the initial improvements to the mock-up could be to include the high explosives surrounding the tamper and a surrounding case. Expanding the model to include a complete sphere instead of a hemisphere would improve the validity of the results, as would purchasing, or manufacturing, models using materials as close to the actual weapon as feasible would improve the accuracy and reliability of the results obtained.

A numerical model is critical to thorough research in modeling a warhead or a spoof. A numerical model would allow for research of different research isotopes, such as I-131, to be used

within the distributed source. Additional capabilities to account for self-shielding of the source and build-up factors from real geometry need to be incorporated into the model. The model should also allow for different materials and thickness of material to be used in the reflector, tamper, high explosives, and weapon's case. Other model options could include a complete sphere and incorporation of additional surrounding materials to simulate a storage container and associated packing.

The three regions of the plutonium gamma spectrum should be specified for investigation. The first region would be ≤ 200 keV. This region would be used to identify spoofs not capable of attenuating the low energy gammas and for baseline calibration purposes. The 159 keV peak obtained from Te-123m would work well as a point source since it is near the 160 keV peak associated with Pu-241 and Pu-240. The second range would be ≥ 200 keV and ≤ 500 keV. The 392 keV peak from Sn-113 along with several gamma peaks from Eu-152 would provide a good point sources while I-131 may be available from hospital suppliers to use as a distributed source. Plutonium peaks of interest in the region include 375 keV peaks and the 413 keV peak and americium has peaks in this region. The remaining region would be ≥ 500 keV. The peaks of interest have been covered extensively in other portions of this project. Appropriate point sources and distributed sources include the Cs-137 sources already discussed. Requirements for any mock-up experiments should include WGPu if possible. At a minimum, RGPu in better geometry should be obtained.

Appendix A Key Gammas

Table 10 through Table 13 list the key gammas for the nuclides of interest in SNM detection: U235, U-238, Pu-239, and Pu-240. The gammas listed are those that have a 1:100,000 chance, or better, of occurrence. Only one Pu-238 gamma (766 keV) escapes the SNM container and is of such small concentration that is not used in WGPu identification. No Pu-241 or Pu-242 gammas escape the SNM package and can not be used in WGPu identification.

Table 10 U-235 key gammas

Nuclide	Energy (keV)	Yield (%)	Rate [gammas/(sec*gram)]
U-235 T½ = 7.038E+8 Years Alpha+Gammas Specific Activity = 8.00E+4 Bq/gram	13.00	51.00	4.08E+4
	19.59	61.00	4.88E+4
	72.70	0.110	88
	89.9530	3.56	2848
	93.3500	5.81	4648
	94.0	0.400	320
	95.70	0.19	152
	105.0	2.69	2152
	109.160	1.54	1232
	140.76	0.220	176
	143.760	10.96	8768
	163.330	5.08	4064
	182.61	0.340	272
	185.715	57.2	4.576E+4
	194.940	0.630	504
	202.110	1.080	864
	205.311	5.01	4008
	221.380	0.120	96

Table 11 U-238 key gammas

Nuclide	Energy (keV)	Yield (%)	Rate [gammas/(sec*gram)]
U-238 T½ = 4.468E+8 Years Alpha+Gammas Specific Activity = 1.24E+4 Bq/gram	13.00	8.0000	992.0
	49.55	0.0640	7.936
	89.9530	0.00070	0.0868
	93.3500	0.00114	0.14136
	105.00	0.00053	0.06572
	113.50	0.0102	1.2648

Table 12 Pu-239 key gammas

Nuclide	Energy (keV)	Yield (%)	Rate [gammas/(sec*gram)]
Pu-239 T½ = 24,110 Years Alpha+Gammas Specific Activity = 2.29E+9 Bq/gram	12.97	0.01840	4.23E+5
	13.60	4.90000	1.13E+8
	30.04	0.00022	4.99E+3
	38.66	0.01050	2.42E+5
	42.06	0.00017	3.80E+3
	46.21	0.00074	1.70E+4
	46.69	0.00006	1.33E+3
	47.56	0.00006	1.29E+3
	51.62	0.02710	6.23E+5
	54.04	0.00020	4.53E+3
	56.83	0.00113	2.60E+4
	65.71	0.00005	1.06E+3
	67.67	0.00016	3.77E+3
	68.70	0.00030	6.90E+3
	68.74	0.00011	2.53E+3
	77.59	0.00041	9.43E+3
	78.43	0.00014	3.24E+3
	94.67	0.00380	8.74E+4
	96.13	0.00002	5.06E+2
	97.60	0.00008	1.84E+3
	98.44	0.00610	1.40E+5
	98.78	0.00122	2.81E+4
	103.06	0.00023	5.29E+3
	111.00	0.00290	6.67E+4
	115.38	0.00046	1.06E+4
	116.26	0.00060	1.37E+4
	119.72	0.00002	5.06E+2

	Energy (keV)	Yield (%)	Rate [Gammas/(sec*gram)]
	123.62	0.00002	4.60E+2
	124.51	0.00006	1.40E+3
	125.21	0.00007	1.63E+3
	129.30	0.00631	1.45E+5
	141.66	0.00003	7.36E+2
	143.35	0.00002	3.98E+2
	144.20	0.00028	6.51E+3
	146.09	0.00012	2.74E+3
	161.45	0.00012	2.83E+3
	171.39	0.00011	2.53E+3
	179.22	0.00007	1.52E+3
	188.23	0.00001	2.53E+2
	189.36	0.00008	1.91E+3
	195.68	0.00011	2.46E+3
	203.55	0.00057	1.31E+4
	225.42	0.00002	3.47E+2
	237.77	0.00001	3.31E+2
	243.38	0.00253	5.82E+4
	255.38	0.00008	1.84E+3
	263.95	0.00003	6.21E+2
	297.46	0.00005	1.15E+3
	311.78	0.00003	5.93E+2
	316.41	0.00001	3.04E+2
	320.86	0.00005	1.25E+3
	323.84	0.00005	1.24E+3
	332.85	0.00049	1.14E+4
	336.11	0.00011	2.58E+3
	341.51	0.00007	1.52E+3
	345.01	0.00003	5.75E+2
	345.01	0.00056	1.28E+4
	361.89	0.00001	2.81E+2
	367.07	0.00009	2.05E+3
	368.55	0.00009	2.02E+3
	375.05	0.00155	3.57E+4
	380.19	0.00031	7.02E+3
	382.75	0.00026	5.96E+3
	392.53	0.00021	4.72E+3
	393.14	0.00035	8.05E+3
	413.71	0.00147	3.37E+4
	422.06	0.00012	2.81E+3
	451.48	0.00019	4.35E+3
	645.94	0.00002	3.50E+2

Table 13 Pu-240 key gammas

Nuclide	Energy (keV)	Yield (%)	Rate [gammas/(sec*gram)]
Pu-240 T½ = 6564 Years Alpha+Gammas Specific Activity = 8.43E+9 Bq/gram	13.60	11.0000	9.27E+08
	45.24	0.04500	3.79E+06
	94.67	2.65E-05	2.23E+03
	98.44	0.000043	3.62E+03
	104.23	0.00708	5.97E+05
	111.00	0.00002	1.69E+03
	160.31	0.000402	3.39E+04
	212.46	0.000029	2.44E+03
	642.35	0.000013	1.10E+03

Gamma Energies, half-life, and yield (%) data taken from Brookhaven National Laboratories website (4). Specific activity calculated from the equation below:

$$SA = \frac{\ln(2) * Av}{T^{1/2} * M}, \tag{13}$$

where SA is the specific activity in Bq per gram, Av is Avogadro's number, $T^{1/2}$ is the half-life in seconds, and M is the molecular weight in grams (16:2)

Appendix B Mass Attenuation Coefficients

Many materials were investigated for possible use as the reflector and the tamper in addition to the material shown in the Fetter model. Reflector materials that could be have been used as substitutes for Beryllium included carbon (graphite) and the hollow aluminum hemisphere that was chosen. Possible filling for the aluminum shell included silica, alumna, and graphite before water was chosen. Lead was the only substitute considered for a fitting substitute for the uranium/tungsten tamper.

Cyclonite, trimethylene trinitramine, $(CH_2)_3N_3(NO_2)_3$, was chosen for attenuation calculations for the high explosive. Had the model developed to the point of using the surrounding high explosives, paraffin would have been a good substitute. Aluminum would have been used as the casing material had the project developed to that stage.

Figure 37 to Figure 38 show the mass attenuation coefficients for a high Z material and a low Z material, respectively. The mass attenuation coefficients data used throughout the project can be found on the NuDat website (4).

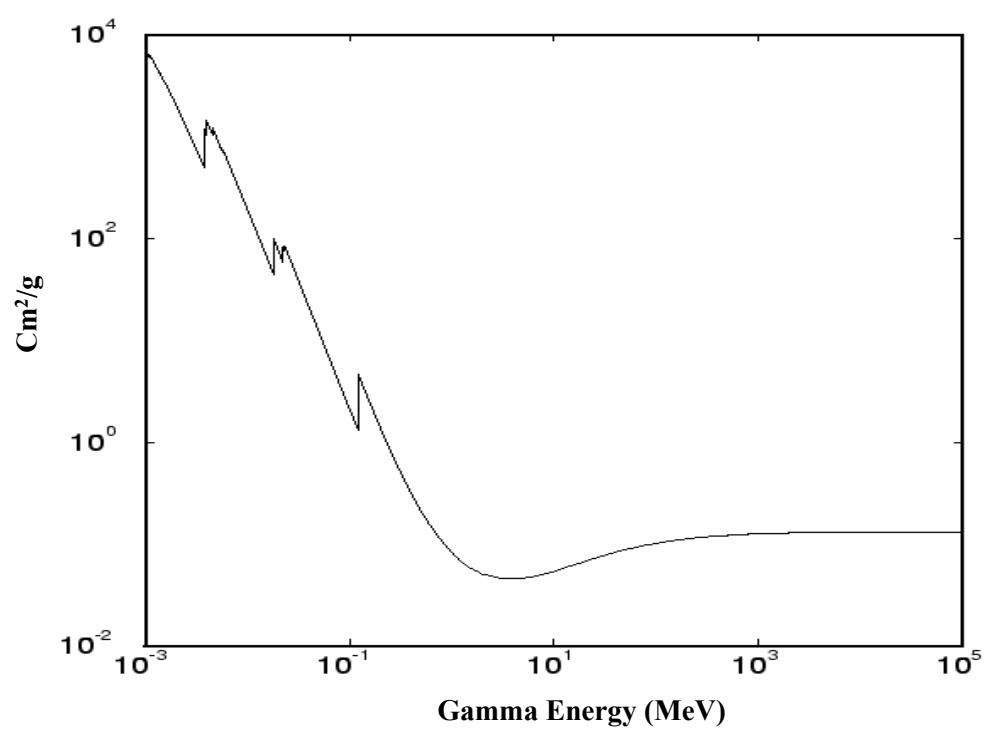

Figure 37 Example of mass attenuation coefficient curve for a high Z material (Plutonium)

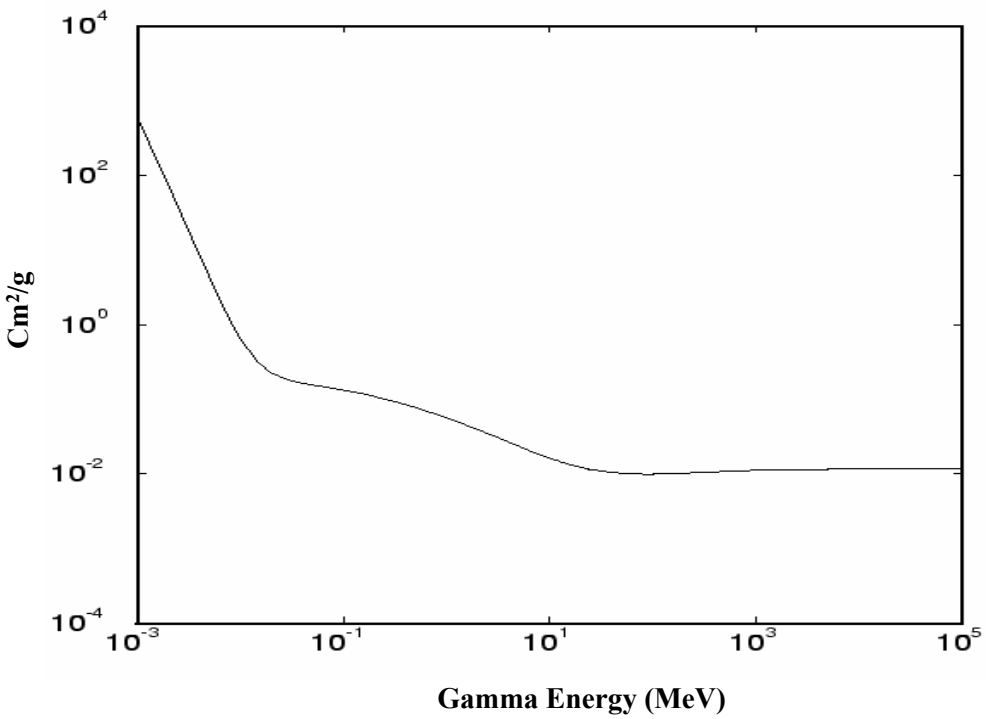

Figure 38 Example of mass attenuation coefficient curve for a low Z material (Beryllium)

Appendix C Weapon Mock-Up

A hollow polymer bowl was constructed to hold a Cs-137 source suspended in a 1M HCl solution. This substitute for the pit was placed inside a hemispherical aluminum shell filled with water. The aluminum shell served as a substitute for the reflector in the Fetter model shown earlier. The outer shell consisted of a hemispherical shell constructed from lead. This shell served as a substitute for the tamper in the Fetter model.

The bowl was constructed from a polymer with a specific gravity of 1.28 gm/cm^3. The outer and inner surfaces along with the end cap are 0.3 inches (7.62 mm) thick surrounding a hollow cavity constructed to be 0.3 inches (7.62 mm) across. The bowl contained a Cs-137 source suspended in approximately 54 ml of 1M HCl. The bowl, in testing configuration, is shown in Figure 39.

Figure 39 Distributed Cs-137 bowl source in testing configuration

The reflector consisted of a spun aluminum shell approximately 1 mm thick with a total thickness of approximately 2.54 cm. In order to have the approximate effect of the beryllium shield, the shell was filled with water. The reflector, fitted over the source bowl, is shown in Figure 40.

Beryllium acts primarily as an absorber that allowed 77.6% of the gammas (*N*) from the 662 keV a Cs-137 source to pass through as calculated in the following equation

.

$$N = N_o e^{-\frac{\mu}{\rho}\rho x} . \qquad (14)$$

Where N_o is initial number of gammas emitted (set to one for percentage calculations), μ/ρ is the mass attenuation factor (cm^2/gm), ρ is the density (gm/cm^3), and x is the thickness (cm) of the reflector in the Fetter model. The options for materials to use to fill the aluminum shell included alumina, silica, and water. Alumina and silica only allowed 60.1% and 63.8% of the gammas rays of interest pass while water allowed 77.3% of the gammas of interest to pass through the reflector. The best match proved to be water, with a difference of only –0.3% compared to –16.5% and –13.8% respectively.

Figure 40 Simulated reflector consisting of a water filled aluminum hemisphere in testing configuration

The thickness of lead required for the mock-up was based upon an average between the depleted uranium tamper and the tungsten tamper shown in the Fetter model. The get the same scattering effect in the mock-up, it was determined that 4.04 cm would be required. Because of material constraints, the tamper was made from poured lead using an aluminum mold. The inner mold consisted of the aluminum shell already discussed and the outer mold consisted of the next larger aluminum shell from the same previous experiment. The lead was approximately 2.54 cm instead of the 4.04 cm calculated. The lead shield can be seen in its testing configuration, covering the source and reflector, in Figure 41.

Figure 41 Simulated lead tamper in testing configuration

Appendix D Sources and Source Activity

The following equation converts the initial activity of radioactive sources to the activity used during the experiments

$$A = A_o \exp((-\ln 2/T)t) \tag{15}$$

where A is the current activity (Bq or Ci), A_o is the initial activity (Bq or Ci), T is the half-life, and t is the time between activity A and A_o. The sources used throughout the experiment are shown in Table 14.

Table 14 Sources used in the experiment

Source (Date Activated)	Nuclide in the source	Initial Activity (uCi)	Half-life
Multinuclide Standard Source T105, Isotope Products Laboratories, Source Number 947-77 (1 Nov 2002)	Am-241	0.1522	432.17 years
	Cd-109	1.400	462.6 days
	Co-57	0.05457	271.79 days
	Te-123m	0.06895	119.7 days
	Cr-51	1.836	27.706 days
	Sn-113	0.2530	115.09 days
	Sr-85	0.3509	64.849 days
	Cs-137	0.2365	30.17 years
	Y-88	0.5066	106.630 days
	Co-60	0.2840	5.272 years
	Co-60	0.2840	5.272 years
	Y-88	0.5066	106.630 days
Am-241--Source 17, Amersham, Source Number 1Q701 (31 May 1982)	Am-241	11.83	432.17 years
Cs-137—Source T089, Isotope Products Laboratories, Source Number 619-44-2 (1 Aug 1998)	Cs-137	10.02	30.17 years

Cs-137—Source 133, Amersham, Liquid Source, (31 May 1981)	Cs-137	1100	30.17 years
Co-57—Source T085, Isotope Products Laboratories, Source Number 619-42-1 (15 Aug 1998)	Co-57	94.03	271.79 days
Pu-239—Source 296, Hickmott, Source Number 9/10 (28 Feb 1981)	Pu-239	12,000	24,110 years
U-235/U-238—Source 413, Natural Ore (21 Mar 1993)	U-235 / U-238	0.081 / 7.65	7.038E+8 years / 4.468E+8 years
Cs-137—Source 133A, AFIT, Liquid Source, (10 Jan 2003)	Cs-137	650	30.17 years

The plutonium source consisted of two metal cylinders approximately 6 mm in diameter and 3 mm thick. Each cylinder remained within its own glass vial. The mass of the plutonium was calculated to be 0.192 grams using the equation below (16:2)

$$mass = \frac{A * M * T^{1/2}}{Av * \ln(2)}. \tag{16}$$

A is the activity in Bq, M is the molecular mass in grams per mole, $T^{1/2}$ is the half-life in seconds, and Av is Avagadro's number. The calculation was based upon the assumption that the recorded activity is for pure Pu-239 as listed in AFIT's radioactive source records.

Appendix E Solid Angle Approximations

This appendix shows the solid angle approximation and equations used in the experiments conducted throughout this project. A point source that emits radiation isotropically is used to determine the solid angle. A cone, as shown in Figure 42, is projected from the source and intersects an imaginary sphere surrounding the source, which defines the solid angle.

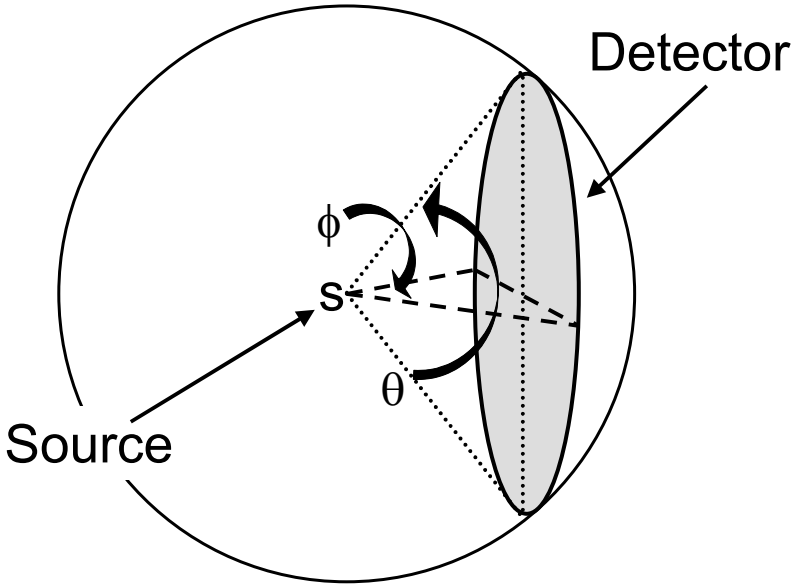

Figure 42 Geometry configuration for a point source approximation of the solid-angle

The solid angle, Ω (steradians), can be expressed as,

$$\Omega = \int_0^{2\tan^{-1}\left(\frac{a}{d}\right)} \int_0^{2\tan^{-1}\left(\frac{a}{d}\right)} \sin(\theta) d\theta d\phi \,, \tag{17}$$

where *a* is the radius of the source, *d* is the distance from the source to the detector, ϕ is the horizontal angle, and θ is the vertical angle.

In order to be more accurate, the approximation can be modified to model the source as a uniform disk with a radius *s* as shown in Figure 43. When making this modification, Equation 17 must be modified to include the new source geometry.

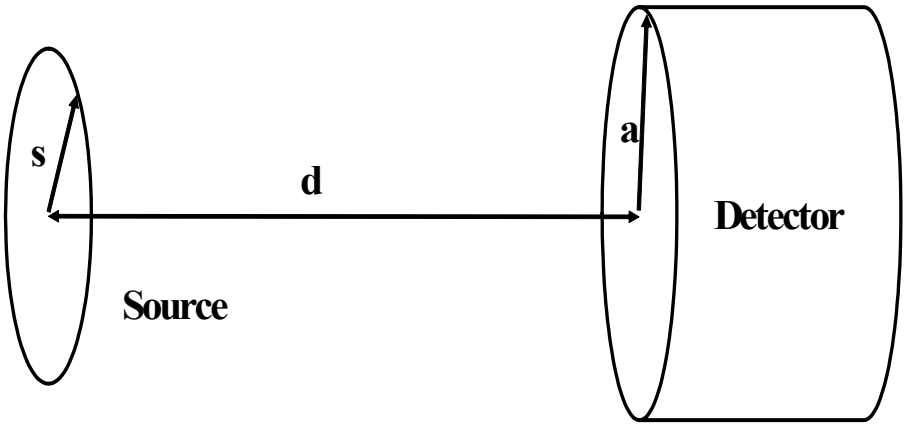

Figure 43 Solid-angle geometry for a uniform circular disk incident on a circular detector and aligned on a central axis

The additional term below defines the average solid angle subtended by the detector across the surface of the uniform disk source. The solid angle for a distributed source is defined as

$$\Omega = \int_0^S \int_0^{2\tan^{-1}\left(\frac{a}{d}\right)} \int_0^{2\tan^{-1}\left(\frac{a}{d}\right)} \sin(\theta) \frac{\cos\left(\tan^{-1}\left(\frac{s`}{d}\right)\right)}{s} d\theta d\phi ds`, \qquad (18)$$

where the additional term, s', is the radius of the distributed source that is being integrated while *s* is the radius of the uniform disk source.

An order of magnitude check on the solutions obtained from the above calculations was made with the approximation for the point source equation below,

$$\Omega = 2\pi(1 - \frac{d}{\sqrt{d^2 + a^2}}), \tag{19}$$

where d is the distance from the detector to the source and a is the radius of the detector (16:118)

Appendix F Equipment, Equipment Settings, and Detector Specifications

The primary equipment used in the experiments can be found below in Table 15.

Table 15 Electrical equipment listing of modules and detectors used in the project

Item Name	Manufacturer	Model	Serial Number
AIM (1)	Canberra	556A	09028403
AIM (2)	Canberra	556	09932142
AIM (3)	ND	556	09932150
(Spectroscopy) Amplifier (1)	Canberra	9615	06027140
(Spectroscopy) Amplifier (2)	Canberra	9615	06027143
Spectroscopy Amplifier (3)	ORTEC	672	334
ADC (1)	Canberra	8701	07027656
ADC (2)	Canberra	8701	07027658
ADC (3)	Canberra	9633	01017260
HVPS (1)	Canberra	9645	08027948
HVPS (2)	Canberra	9645	08027950
HVPS (3)	ORTEC	659	235
Modular System Bin (1)	ORTEC	4001A	6315
Modular System Bin (2)	ORTEC	4001A	6306
Modular System Bin (3)	ND	0089	1 of 4 (local ID)
Modular System Bin (3)	ND	0089	2 of 4 (local ID)
NIM Bin Power Supply (1)	ORTEC	4002D	3279
NIM Bin Power Supply (2)	ORTEC	4002D	3278
NIM Bin Power Supply (3)	ND	880756	880061
NIM Bin Power Supply (3)	ND	880756	880064
HgI_2 Detector	Constellation*	MMOD-025-001.04	00609N15
Preamplifier of HgI_2	Constellation*	MMOD-025-001.04	PR-355 0119
EMC HPGe Detector	ORTEC	GEM-50195-P-S	40-TP31441A
Preamplifier of EMC HPGe	ORTEC	257P	468
LN_2 HPGe Detector	ORTEC	GMX-20195	26-N-08PB
Preamplifier of LN_2 HPGe	ORTEC	257N	647 Rev 1

*Constellation Technology Corporation
(1) Used with the HgI_2 Detector System
(2) Used with the EMC HPGe Detector System
(3) Used with the LN_2 HPGe Detector System

The experiments used the following settings.

a. HgI_2 Detector Setup

1) Constellation HgI_2 detector. Model-MMOD-025-001.04, 10 mm x 10 mm x 1.67 mm crystal.

    Source Height-8 cm, centered over the crystal

2) Canberra Model 556A Acquisition Interface Module.

    ID Number: 0E99

3) Canberra Model 8701 Analog –Digital Converter

    Range: 2048
    Gain: 2048
    Offset: None
    Peak Detect: Auto
    PHA/SVA: PHA
    COINC/ANTI: Coinc

4) Canberra Model 9615 (Spectroscopy) Amplifier

    Preamp type: RC
    Coarse gain: 10
    Fine gain: 2.5555x
    S-fine gain: 1.00085x
    Amp gain: 25.5768
    Shaping (us): 12
    Shaping mode: Gaussian
    Input mode: Normal
    Inp. Polarity: Positive
    BLR mode: Sym
    Inh. polarity: Positive
    LTC mode: Normal
    PUR: On
    Pole zero: 539

5) Canberra Model 9645 High Voltage Power Supply

Voltage: 1700.88V
Over. latch: Enabled
Inh. latch: Enabled
Inh. signal: 5V
Polarity: Positive
Inhibit: Clear
Overload: Clear
Status: On

b. EMC HPGe Detector Set up

1) ORTEC HPGe Detector. Model-GEM-50195-P-S, Electromechanically Cooled by Stirling engine. System configured by Constellation, 70.0 mm x 58.4 mm crystal.

Source Distance-30 cm, centered over the crystal

2) Canberra Model 556 Acquisition Interface Module.

ID Number: 050D

3) Canberra Model 8701 Analog –Digital Converter

Range: 8192
Gain: 8192
Offset: None
Peak Detect: Auto
PHA/SVA: PHA
COINC/ANTI: Coinc

4) Canberra Model 9615 (Spectroscopy) Amplifier

Preamp type: RC
Coarse gain: 10
Fine gain: 5.000x
S-fine gain: 1.00001x
Amp gain: 7.50006
Shaping (us): 12
Shaping mode: Gaussian
Input mode: Normal
Inp. Polarity: positive
BLR mode: Sym
Inh. polarity: Positive
LTC mode: Normal
PUR: Off
Pole zero: 2816

5) Canberra Model 9645 High Voltage Power Supply

Voltage: 2498.53V
Over. latch: Enabled
Inh. latch: Enabled
Inh. signal: 5V
Polarity: Positive
Inhibit: Clear
Overload: Clear
Status: On

c. LN_2 HPGe Detector Set up

1) ORTEC HPGe Detector. Model-GMX-20195, 50.0 mm x 55.0 mm crystal, hole dimension 9.3 mm x 4.72 cm

Source Distance-0.5 cm, centered over the crystal (for calibration)
Source Distance-15.9 cm, centered over the crystal (Pu source)

2) Canberra Model 556 Acquisition Interface Module.

ID Number: 0501

3) Canberra Model 8701 Analog –Digital Converter

Transfer Timing: Overlap
Peak Detect: Auto
Coinc Mode: Coinc
Acq. Mode: PHA
Range: 16384
Conv. Gain: 16384
Offset: 0
LLD: 3.03 %
ULD: 110 %
Zero: 0.001 %
LTC/PUR sig: LG

4) Canberra Model 9615 (Spectroscopy) Amplifier

FG: 10
CG: 20
UNI Shaping: Gaussian
PA: Auto
Shaping (us): 2
BLR : PZ
Input: Normal (-)

5) Canberra Model 9645 High Voltage Power Supply

Voltage: - 3000V
HV: On

The specifications of the HgI_2 detector, EMC HPGe detector, and the LN_2 HPGe detectors are shown in Table 16, Table 17, and Table 18 respectively.

Table 16 HgI_2 detector specifications

Specification	Data
Case Size	89 mm x 51 mm x 51 mm
Crystal Size	
Weight	230 grams
Electrical power requirements	+6 to +14 VDC, < 10mA

Table 17 EMC HPGe detector specifications

Specification		Data
EMC and detector	Size	20 cm x 21.5 cm x 57 cm to end of cold finger with coaxial detector: 84 cm
	Weight	16.8 kg (50% coaxial HPGe)
	Mounting	4 rubber feet
Transport Case	Size	91 cm x 46 cm x 36 cm
	Weight, with EMC	44 kg (23 kg empty)
Electrical power requirements, 12 VDC		Cooling: 180 watts
		At operating temperature: 90 watts at EMC
Operation on internal transport case battery		Usable EMC operation: 40 min
		Recharging time: 3 hours
Operation on external DC power		16 amps maximum
Cooling time from room temperature		8 hours
Detector Type		Modified ORTEC Pop-Top™
Ambient operating temperature		-20°C to + 40°C
Mounting		Detector axis horizontal
Humidity		Non-condensing

Table 18 LN_2 HPGe detector specifications

Specification		Data
Detector	Crystal Size	50 mm x 55 mm
		50% coaxial HPGe
Cooling time from room temperature		6 hours
Detector Type		ORTEC GMX Series Gamma-X
Ambient operating temperature		-20°C (LN_2-cooled)
Mounting		Detector axis horizontal

Appendix G Protocol Procedures

This appendix includes the protocol procedures and the steps followed in the transfer of the bowl source. The exposure rate of the original source was determined with the assumptions listed in Knoll (16:58-9). The following equation was used to calculate the exposure rate:

$$\dot{X} = \prod_{\delta} \alpha / d^2 \tag{20}$$

where $\dot{X}$ is the exposure rate in R/hr, *d* is the distance from the source in cm, α is the activity of the source in mCi, and Γ_δ is the exposure rate constant in (R*cm^2/mCi*hr). The values for the Cs-137 source used in this experiment were:

Table 19 Protocol exposure rates from the liquid source used to make the distributed source

Distance from the Source	Calculated Value	Measured Value
1 cm	2208	44
30 cm	2.43	2.9
50 cm	0.833	1.24
Background	N/A	0.090

The geometry of the detector and the geometry of the source resulted in the discrepancy in the one cm measurement. As the source got very close to the detector, it no longer appeared as a point source to the detector and self-shielding of the source showed the reading actually received as a body dose. The higher number is the total dose rate given off by the source.

The activity of the source during the transfer was 0.669 mCi and the value of Γ_δ is 3.3 R*cm^2/mCi*hr for a Cs-137 source (16:59).

Safety Protocol: Gamma Spectroscopy and Imaging Experiments

A. Background

1. Title of experiment: Gamma Spectrometry Experiments

2. Principal investigators: Dr Larry Burggraf and LTC James Petrosky

Location: Bldg 470 Basement Lab and Instrumentation Lab

3.Personnel involved: Current Master's Student: MAJ Michael Nelson

Former Students: Capt Brian Evans, Mr Mathew Lange, and MAJ Thomas Cartledge

Faculty Advisor: Dr. Burggraf and LTC Petrosky

B. Description of experiment: Gamma spectrometry and imaging involves measurement of photoelectric absorption and Compton scatter of gammas in arrays of a variety of materials. These material arrays simulate a various DoD applications including nuclear weapons simulators and aircraft structures. Examples of previous studies are:

1. Comparison of Spectral Analysis software (Master's Thesis by MAJ Cartledge

2. Compton backscatter imaging (PhD Dissertation by Capt Evans and MS Thesis by Mr Matthew Lange)

3. NENG 650 Experiments

A new focus of this research is gamma spectrometry and imaging for nuclear weapon simulations. This research uses sealed or encapsulated sources and "open" sources to simulate gamma radiation from nuclear fuels. The work will evaluate a variety of detectors, detection methods and detection scenarios to understand what information is necessary to characterize nuclear weapons by means of gamma radiation that may be emitted.

For example, recent studies show that electromechanically cooled high purity germanium (HPGe) detectors may be viable replacements for LN_2 cooled HPGe detectors as well as HgI_2 detectors as a possible replacement for NaI(Tl) room temperature detectors. Gamma Spectroscopy experiments will examine the response functions and capabilities of solid-state detectors to characterize point gamma sources (sealed or encapsulated) and distributed sources (open). Gamma measurements will be conducted in the B470 Basement Laboratory and in the B470 Instrumentation Laboratory. Distributed sources will be prepared from radioisotope solutions, initially Cs-137, using standard methods for handling "open" sources. Sealed gamma sources and "open" gamma sources will be used exclusively in Bldg 470.

Experimental procedures: Encapsulated sources will be placed in assorted arrangements as mock-ups of nuclear weapons or Special Nuclear Material (SNM) containers. Gamma spectroscopy measurements will be made using LN_2 cooled HPGe detectors, an electromechanically cooled HPGe detector and various room temperature solid state detectors, including a mercuric iodide detector. Distributed sources, usually acidic liquid solutions of radioisotopes such as Cs137, will also be measured using various configurations of absorbers and scattering materials. For example, initial work will examine the photoelectric and Compton scatter effects from a SNM package mock-up.

Equipment used:

1. Standard spectroscopy electronics to include:

    a) AIM

    b) (Spectroscopy) Amplifier

    c) High Voltage Power Supply (6 kV maximum)

    d) Analog-Digital Converter

e) PC-based Multichannel Analyzer

2. Gamma radiation detectors to include:

a) LN_2 cooled HPGe

b) Electromechanically cooled HPGe

c) NaI(Tl) and CsI(Tl) scintillation detectors

d) HgI_2 and CZT room temperature solid state detectors

3. Gamma sources: encapsulated and "open" sources with typical activity in the range from 10 to 1000 microcuries.

4. Other equipment includes weapons mock-up constructed from polymer-based material to contain suspended "open" source, and absorbing/scattering element made of aluminum, lead, etc.

C. Summary of major safety issues: Potential hazards are from:

1. Radioactive sources: Wipe/Leak tests to be conducted on both the exterior of the old and new containers. Additionally, wipe tests will be conducted on the table under the hood where the samples are transferred. Containers for all materials such as gloves and the pipette used in the transfer of the source will also be wipe tested. Wipe tests and radiation measurements will be used as an indication of whether LLR wastes have been created.

2. High Voltages for Radiation detectors.

3. Chemical compounds (such as HCl) used to suspend the sources. Some chemical preparations, using radioisotopes, will be conducted in B644.

4. Standard office hazards

D. Detailed safety analysis

1. Chemicals used:

a) Typical chemicals: 1 M HCl to suspend a Cs-137 distributed source

b) Typical exposure rate: gamma exposure from Cs-137 source, Local ID# 00133, activity as of 28 October 2002: 670.797 μCi.

1) 2208 mR/hr on contact (calculated)

2) 2.9 mR/hr at 30 cm (measured)

3) 1.24 mR/hr at 50 cm (measured)

4) 0.090 mR/hr background

2. Location/quantity of stored chemicals:

a) Storage Location: Bldg 470 Chem Room

b) Small quantities of dilute acids (typically <100mL)

3. Hazardous waste generated:

Radiation waste:

a) Pipettes, droppers, tweezers

b) Radioactive specimen container

c) Latex gloves

d) Adsorbent pads

Chemical waste: none

4. Ventilation requirements: Radioisotope chemical hood for transfer of radioactive sample require normal room ventilation.

5. Electrical hazards:

a) 10 V AC for all electrical equipment.

b) Up to 3000 V power supplies for radiation detectors; no exposed leads; all connections are with shielded and insulated coaxial cables.

6. Laser hazards: None

7. Ionizing radiation:

a) Various alpha, beta and gamma sources on the ENP radioisotope inventory

b) Cs-137 source, Local ID# 00133, Activity as of 28 October 2002: 670.797 μCi and similar sources.

8. Other safety or bioenvironmental hazards: None

9. Available protective equipment:

a) Dosimetry badges for whole body and fingers

b) Gamma survey meters, hand/feet radiation monitors and GM survey meter.

c) Safety glasses, lab coats, tongs, gloves

10. Other protective equipment required: None

11. Exposure monitors/alarms/detectors: See 9.

12. Emergency plans/procedures: As described in WPAFB Reg 40-201 and summarized in Departmental document on Radiation Safety Training for AFIT Students and Faculty.

13. Limitations currently imposed by safety requirements: None

14. Recommendations for improving safety conditions: Working telephone in basement of Bldg 470 for use in emergency.

15. Training recommendations: Training up to date.

16. Questions

a) Have all personnel completed a laser eye examination? Not required.

b) Is a current AF Form 55 filed for all personnel? Yes

c) Have all personnel received CPR training? No

d) Are appropriate MSDS's available? Yes

Procedures for Preparing Hemispherical Cs-137 Source

Step1: Prior to opening the currently sealed source number 00133, 0.67 mCi Cs-137 solution (1M HCl) all materials to be used in the procedure will be properly laid out and in place. Refer to the attached figure below. Items to be labeled include:

a. Radiation waste container (plastic bag with the opening rolled over the edge of its support container)

b. Radiation support container (Plastic beaker, this item will NOT be considered radiation waste IF swipe tests at the end of the operation are negative.)

c. New source closed hemispherical container (hereinafter referred to as the "bowl"), source number 00133A.

d. Transfer tools to include beakers, tweezers, needle nose pliers and screwdriver.

Step 2: The volume of solution contained by the bowl will be determined to know the total volume of solution that may be added without overfill. The bowl will be placed on a cork doughnut or similar support and taped around the center for stabilization support.

Step 3: All personnel involved will wear TLDs to include the finger TLD during the entire operation. Other safety equipment to be worn include:

a. Plastic gloves with the opening rolled down approximately two inches to allow removal without contaminating clothing.

b. Goggles will be worn over the eyes.

c. Lab coats will be worn over clothing.

d. The person actually making the transfer of the radioisotope will wear an apron over the lab coat.

Step 4: Clear plastic will be laid across a portion of the radiation hood surface. This plastic will be covered by chemical wipes to absorb any liquid radiation spills that may occur during transfer. To ensure the paper stays in place, the edges will be taped to the table surface. If necessary, this material will be placed into the radiation waster container upon completion of the transfer operation. (Laboratory absorbent pads will be ordered replace the plastic/paper set-up for future operations).

Step 5: Lead bricks will be placed between the radiation workers and the sample during the operation. Lead bricks will also be placed on the right side of the absorbent pads to provide an uncontaminated, shielded area for monitoring possible contamination of hands.

Step 6: The radiation hoods fan will be running at all times to ensure that any fumes from the HCl are properly vented.

Step 7: The current source container will be fitted into in the small lead "pig" in which it was shipped IAW ALARA procedures. The bottom of the "pig" will have paper towel or similar adsorbent so that the top of the source container will stick up high enough that the metal foil will be clear of the "pig" edge. The piece of towel will be thrown into the radioactive waster upon completion of the operation. The "pig" will be held by hand in order to safely manipulate the removal of the foil and septum.

Step 8: The actual transfer will use the following steps;

a. A small set of needle nose pliers will be used to remove the foil cap on source number 00133. The foil will be placed in the radiation waste container.

b. Vent the sample by pushing a needle through the septum. Place the needle in the radioactive waste container.

c. Tweezers will then be used to carefully remove the septum from the source. The septum will be placed in the radiation waste container. As of this point, the tweezers will be considered radiation waste and placed in the radiation waste container.

d. A plastic dropper will be used to transfer the Cs-137 from the old source container to the bowl. At this point the dropper becomes contaminated will be left in the opening of the bowl when not being used to transfer Cs-137/HCl until completion. Upon completion of the entire transfer operation, the dropper will be placed in the radioactive waste container.

e. A separate plastic dropper will be used to transfer a small amount (approximately 5 ml) of 1 M HCl from the HCl container to the old source container. Care will be used to ensure the dropper does not make contact with the old source container. IF the dropper makes any contact with the old source container it will be disposed of as radioactive waste. If the dropper is not contaminated, it will be returned to the HCl container until it is used again.

f. The dropper from the bowl will now be used to again transfer the contents from the old source container to the bowl.

g. Steps e. and f. will be repeated three times. HCl transfer to the bowl will be continued until the total fill volume has been transferred to the bowl. (The amount of HCl will be pre-measured to minimize the amount of radioactive HCl waste produced in the event of accidental contamination.)

h. Upon completion of the operation, the polyurethane plug will be inserted into the bowl and tightened.

i. Swipes will be taken of the surface of the bowl and tools and the surrounding area to ensure that there is no contamination. If contamination is found, remediation will be done on the contaminated areas and swipes taken again.

j. Swipes will be taken on all surfaces as per standard 88 ABW/EMB Radiation Safety procedures.

Step 8: Upon clearance by 88 ABW/EMB Radiation Safety from the swipe tests, the following steps will be taken:

a. The plug will be slowly tightened into the bowl to minimize effects of building pressure inside the bowl. The edges of the plug will be painted with epoxy for a positive seal.

b. The bowl will be temporarily sealed inside a large, plastic glove box with duct tape for transport to the laboratory.

c. The glove box will be unsealed and the remainder of the weapon mock-up will be placed inside the glove box and the glove box resealed.

d. Anytime the mock-up is not being used in an active experiment, the bowl will be placed under the lead tamper to minimize the dose rate to personnel in the laboratory.

e. The vial that contained the Cs 137 liquid will be monitored for radiation upon completion of the transfer operation.

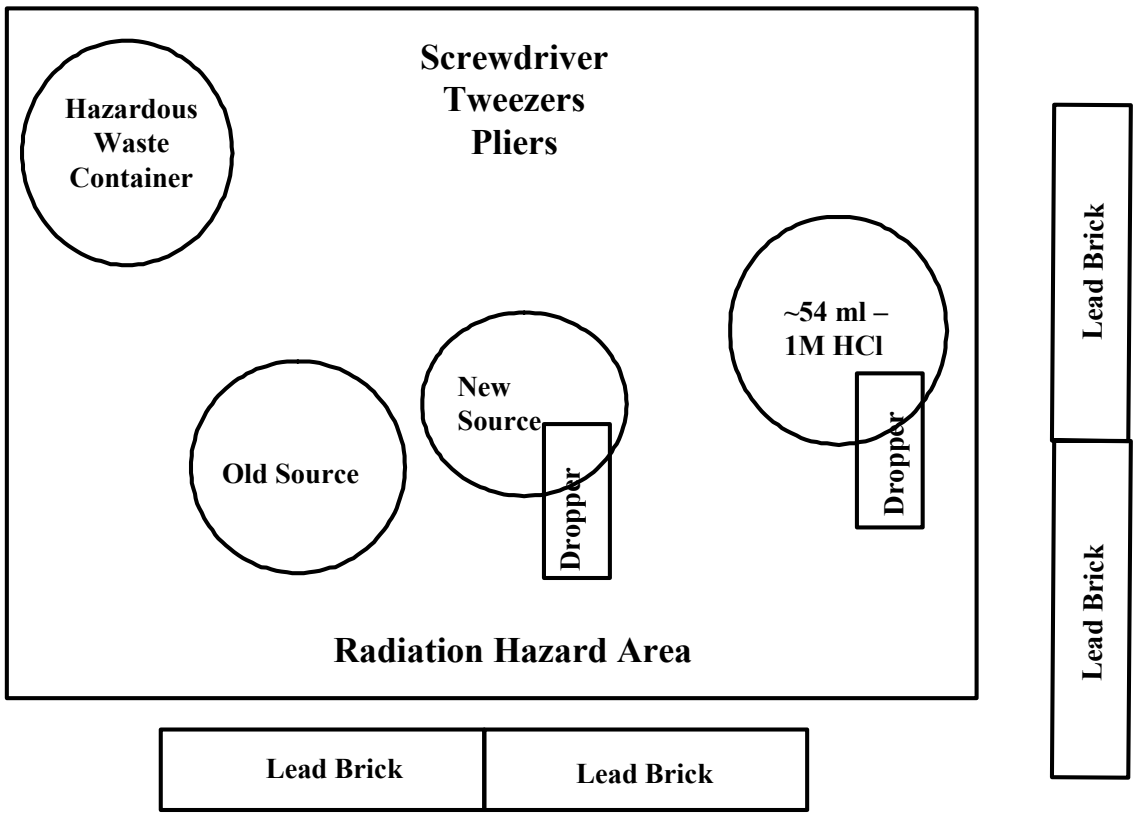

Figure 44 Equipment layout for source transfer under a radiation hood

Recommended Changes to the Protocol

Despite taking the precautions listed in the protocol, the bowl received contamination and had to be remeditated by rinsing with water into a radioactive waste container. In order to eliminate this problem in the future, the following step should be added to the preparation of the new source.

1) Cover the bowl completely with tape or similar item. Upon completion of the transfer, the tape should be carefully removed and placed into the radioactive hazard waste. In this manner, the tape will provide protection from accidental spills and splatter.

2) Use a small, disposable funnel in the mouth of the bowl to minimize spills and splatter.

Appendix H Pu-239 Analysis

This appendix includes the analysis results of the Pu-239 sample used throughout the project. To evaluate the accuracy of the HgI2 and EMC HPGe detectors, the actual composition of the Pu-239 sample has to be determined. A known LN_2 HPGe detector was used to perform the analysis.

Characterize the Source

A 48-hour spectrum (live time) was collected from the AFIT plutonium sample from a distance of 15.5 centimeters centered in front of the axis of the detector. Background was stripped from the sample spectrum to ensure the peaks examined were from the sample and not from the environment. The spectrum collected can be seen in Figure 45.

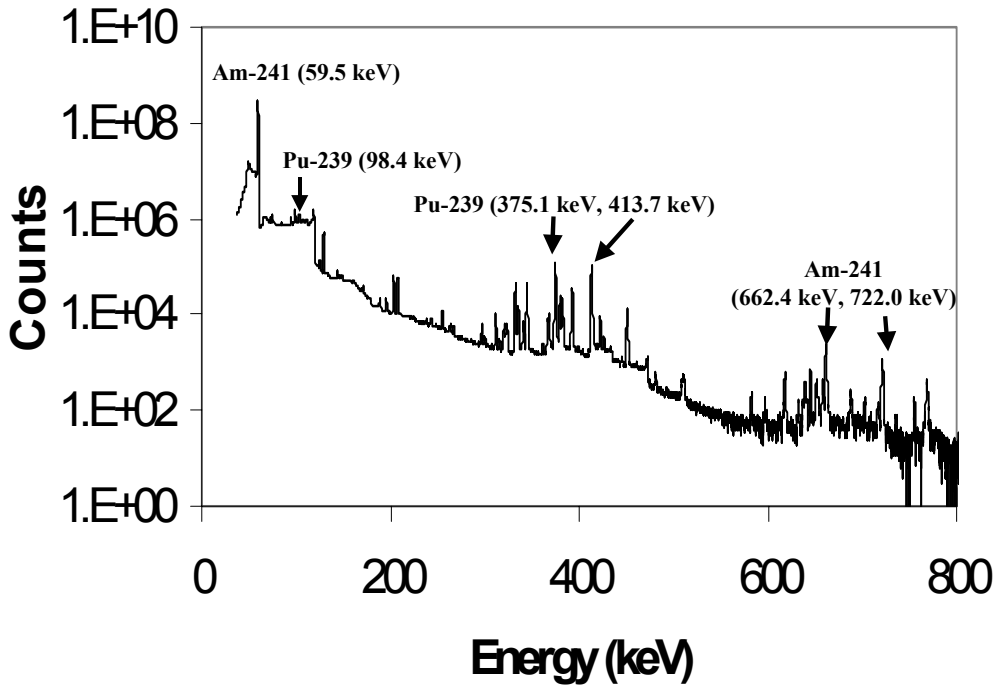

Figure 45 Plutonium spectrum collected for 48 hours from a distance of 15.5 cm using the LN_2 HPGe detector

Figure 46 shows an enlargement of the area of interest for isotopic separation.

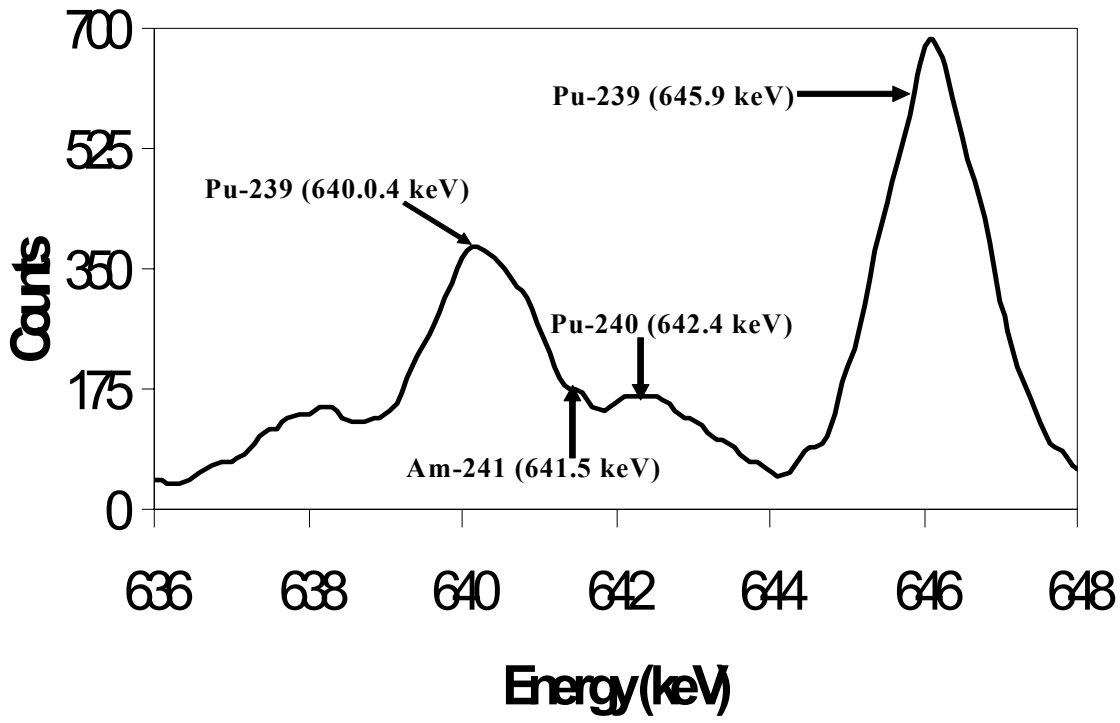

Figure 46 Enlargement of a plutonium spectrum collected for 48 hrs from 15.5 cm using the LN2 HPGe detector. The data is smoothed using a 5-point smoothing routine

Despite a five-point smoothing routine to remove the some of the fluctuations in the spectrum, the Genie 2000 software did not recognize the Pu-240 peak. In addition to the peaks labeled, there are Pu-239 energy peaks at 637.7 and 637.8 keV adding to the Pu-239 640 keV peak. The Pu-239 645.9 keV appeared untainted by overlapping peaks. For this reason the 645.9 keV served as the baseline for all the plutonium peaks.

The total amount of Pu-239 was calculated from the efficiency and branching ratio of the Pu-239 645.9 keV peak. The reverse process was used to determine the area under the remaining Pu-239 peaks in the area of interest. The area under the Pu-240 peak at 642.4 keV was determined by trial and error based upon a ratio between the two plutonium isotopes. An untainted Am-241 peak at

662 keV provided the starting point for the determination of the total Am-241 in the source. Using the branching ratios for Am-241, the area under the 641.4 keV peak in the area of interest was determined. To verify the accuracy of the amount of Pu-239 in the calculations, the amount of Pu-239 was also calculated using the same method, but starting with a Pu-239 peak at 413.7 keV. The results of these calculations, shown in Table 20, verified the value of Pu-239. Attempts to directly calculate the Pu-240 content in isolation failed. Pu-240 does not have an energy peak above background except at energies containing peaks from Am-241, Pu-241, or Pu239.

Table 20 Comparative total amount of plutonium calculated from two different peaks taken in the same spectrum

	413.71 keV Peak	**645.94 keV Peak**
Efficiency (%)	0.028202	0.018182
Specific Activity gammas/(second*gram)	3.50E+02	3.37E+04
Total amount of Pu gammas/(second*gram)	6.752E+8	6.778E+8

The first derivative of the plutonium spectrum is shown in Figure 47. The derivative spectrum emphasizes the changes in the slope of the spectrum. In this manner the maximums and minimums associated with energy peaks can be clearly identified when the slope passes through the primary abscissa. Taking additional derivatives would allow peaks to be further deconvolved as the slope changes at the overlapping edges of the peaks are emphasized. The changes in slope caused by noise and statistical fluctuations in the spectra become more evident with each derivative along with the spectral signal. More derivatives could be taken until the noise becomes too great when compared to the desired spectral signal as seen in Figure 48.

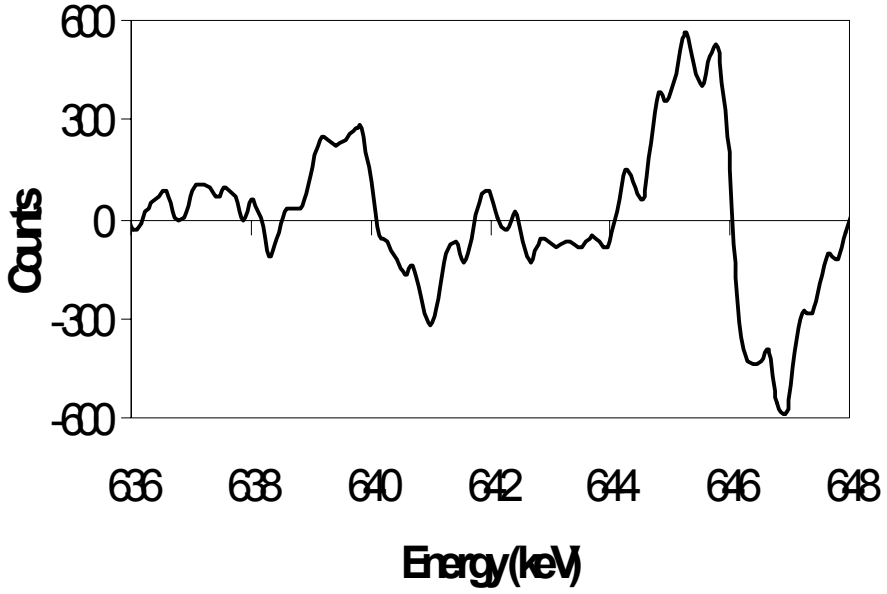

Figure 47 Derivative spectrum of a 640 keV collected for 48 hrs from a distance of 15.5 cm using the LN2 HPGe detector

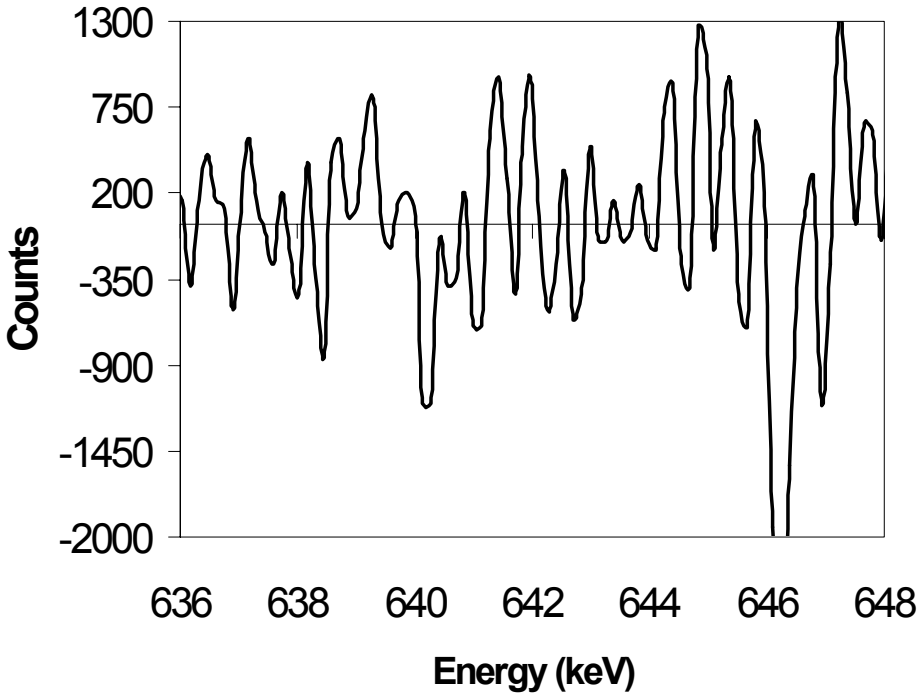

Figure 48 Second derivative spectrum of a 640 keV collected for 48 hrs from a distance of 15.5 cm Using the LN2 HPGe detector

The shape of the simulated peaks was based upon a Cs-137 peak from the efficiency calibration curve. The Cs-137 peak from the calibration curve remained separated from the next nearest peak by almost 150 keV. These conditions ensured the peak shape remained primarily a result of the cesium isotope with little interaction with other peaks. The total counts in the Cs-137 peak were scaled to the value already determined for the plutonium and americium peaks. The 661.7 keV peak from the Cs-137 was then adjusted to the appropriate energy for the plutonium and americium peaks. The assumptions behind this scaling included minimal change in the detector's efficiency over the range of interest, a maximum of 24 keV, and equal bin size throughout the spectrum. The simple sliding of the peak causes negative energy values at the low energy portion of the spectrum. The region of the negative energies is beyond the scope of the project.

Figure 49 shows the simulated spectrum created from the Cs-137 662 keV peak. The scaled spectrum is somewhat larger than the spectrum collected, but fell within the statistical counting variations

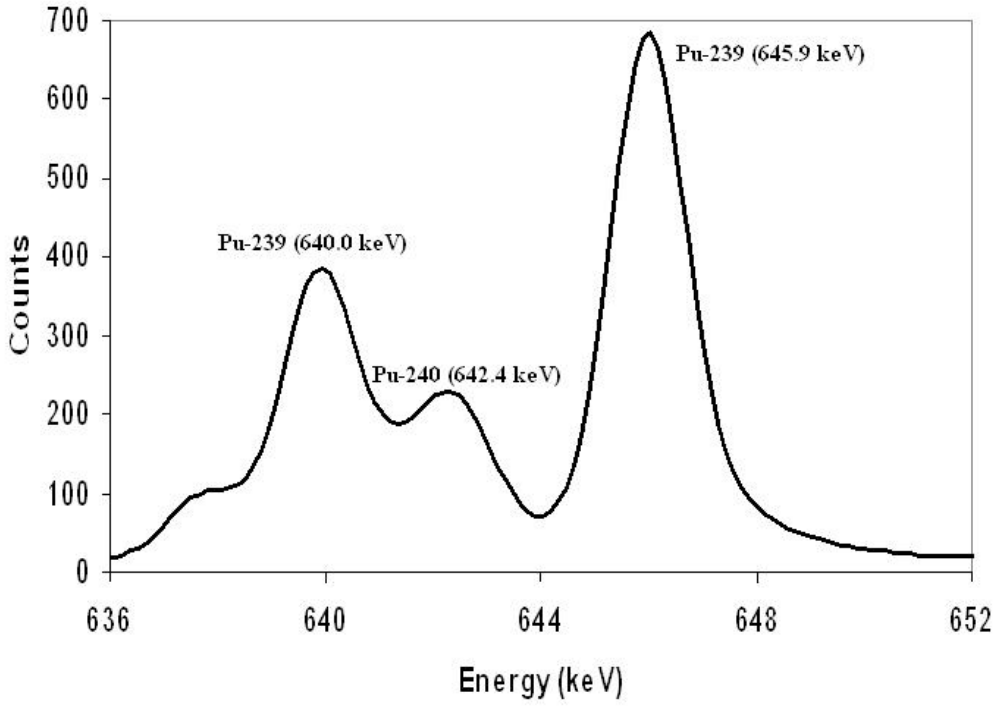

Figure 49 Simulated spectrum created from americium and plutonium peaks in the 640 keV portion of the spectrum

Based upon the data obtained in the deconvolution process, the AFIT Pu-239 source number 296 consisted of fuel grade plutonium with an approximate Pu-239/Pu-240 isotope ratio of 80/20 in addition to small amounts of other elements such as Am-241.

Appendix I Points of Contact

Below is a list of the critical points of contact used throughout this project..

a. Detectors

1) EMC HPGe: Constellation Technology Corporation, 7887 Bryan Dairy Road, Suite 100, Largo, FL 33777-1498. POC: Alan Proctor, email: proctor@contech.com

2) HgI_2: Constellation Technology Corporation, 7887 Bryan Dairy Road, Suite 100, Largo, FL 33777-1498. POC: Kenneth Pohl, email: pohl@contech.com

b. DTRA: LTC Thomas Cartledge, Technology Division, email: Thomas.Cartledge@DTRA.mil

c. Electronics: Canberra Industries Inc., One State Street, Meriden, CT 06450. POC Mr. D. Neville email: dneville@canberra.com

d. Weapon mock-up

1) Distributed source container: Air Force Institute of Technology, Department of Aeronautics and Astronautics, 2950 P Street, WPAFB OH 45433, POC: Jay Anderson, email: Jay.Anderson@afit.edu

2) Lead Shield and Stand: Air Force Institute of Technology, Graduate School of Engineering and Management, 2950 P Street, WPAFB OH 45433, POC: AFIT Model Shop, Bldg 470

e. Source Contamination and Radioactivity Testing: 88th ABW, Radiation Safety Office, WPAFB, OH 45433, POC: Chris Anthony, email: Christopher.Anthony@wpafb.af.mil

Bibliography

1. Berger, M.J., J.H. Hubbell, and S.M. Seltzer, Compilers "XCOM: Photon Cross Sections Database," NIST Standard Reference Database 8 (XGAM) n. pag. http://physics.nist.gov/ PhysRefData/Xcom/Text/XCOM.html. 29 October 2002.

2. Bernstein, Adam, B.A. Brunett, N.R. Hilton, Jim C. Lund, and J.M. Van Scyoc "The 'Radiation Continuity Checker': An Instrument for Monitoring Nuclear disarmament Treaty Compliance," IEEE Transactions on Nuclear Science, vol.49, no.3, June 200, p. 864-9.

3. Berzins, George J., Thomas R., McIlvain, and John Anton, "A Brief Guide of Gamma Detection Systems for Possible Field Applications", Excerpt from unpublished source, 30 December 1999.

4. Burrow, Thomas W. Compiler "National Nuclear Data Center Nuclear Data from NuDat," Excerpt from Brookhaven National Laboratories published data. n. pag. http://www.nndc. bnl.gov/nndc/nudat/ 25 October 2002.

5. Cartledge, Thomas E., DTRA/Technology Applications Division. "Emerging Problems in Arms Control Technology" Electronic Briefing. 4 June 2002.

6. -----. *Comparison of Spectral Analysis Software Programs (RobWin and RSEMCA)*. MS Thesis, AFIT/GNE/ENP/01M-1. Graduate School of Engineering and Management, Air Force Institute of Technology (AU), Wright-Patterson AFB OH, March 2001.

7. -----. "The Ideal Semiconductor Detector," Electronic Mail. 1155L. 12 August 2002.

8. Constellation Technology Corporation. Contract DTRA01-99-C-0187 44-0088-01 with the Defense Threat Reduction Agency. Largo FL, 17 July 2002.

9. Department of Defense. *DoD General Planning Assumptions for Arms Control Treaties and Agreements, FY 02-07* (Coordination Version 2002) Dec 2001.

10. Department of Energy. *Standard DOE-STD-3013-96.* GPO September 1996.

11. Department of Energy. *ACNT : Technology R&D for Arms Control.* California, Spring 2001.

12. Fetter, S., V.A. Frolov, M. Miller, R. Mozley, O.F. Prilutsky, S.N. Rodionov, and R.Z. Sagdeev, "Detecting Nuclear Warheads," in *Reversing the Arms Race: How to Achieve and Verify Deep Reductions in the Nuclear Arsenals*. Ed. F. von Hippel and R.Z. Sagdeev. New York: Gordon and Breach Science Publishers, 1990.

13. *Genie 2000 Operations Manual*. Canberra Industries, Inc., 2001

14. Gilmore, Gordon and John Hemingway, *Practical Gamma Spectrometry* Chichester: John Wiley and Sons, Inc. 2002.

15. Iwanczyk, J.S., W.F. Schnepple, and M.J. Masterson, "The Effect of Charge Trapping on the Spectrometric Performance of HgI2 Gamma Detectors," Nucl. Instr. and Meth., vol.A322, 1992, p. 421-6.

16. Knoll, Glenn F. *Radiation Detection and Measurement* (3rd Edition). New York: John Wiley and Sons, Inc. 2000.

17. Lamonds, H.A. "Review of Mercuric Iodide Development Program in Santa Barbara," Nucl. Instr. and Meth, vol.213, 1983, p. 5-12.

18. Lavietes, A.D., G.J. Mauger, and E.H. Anderson, "Electromechanically Cooled Germanium Radiation Detector System," Nucl. Instr. and Meth., vol.A242, 1999 p. 252-56.

19. Proctor, Alan, Chief Scientist, Constellation Technology Corporation, "RE: Grounding Question." Electronic Message. 11 December 2002.

20. Scheiber, M. R.B. James, J.C. Lund, D.S. McGregor, T.S. Gilbert, J.M. Van Scyoc, R.W. Olsen, and J. Toney, "State of the Art of Wide-Bandgap Semiconductor Nuclear Radiation Detectors," IL Nuovo Cimento, vol. 109A, No. 9, 1996 p. 1253-60.

21. Shleien, Bernard, Lester Slaback, and Brian Birky, *Handbook of Health Physics and Radiological Health, 3rd Edition*. Williams & Wilkins, Baltimore 1998.

22. "Strategic Arms Reduction Treaty (START),"*Arms Control Treaties*. Version 4.0. CD-ROM. Dulles, VA: DTRA, DTRIP Outreach Program Order No. 407X, Mar 2001.

23. "Text of Strategic Offensive Reduction Treaty", Article I, n. pag. http://www.whitehouse. gov/news/ releases/2002/05/20020524-3.html 21 November 2002.

24. Vaccaro, F.P. L. Van den Berg, L.A. Szubert, R.D. Vigil, R.P. DeVito, and C.R. Johnson, "The Long Term Spectral Stability of HgI_2 Gamma Detectors," The Proceedings of SPIE, vol. 4507, 2001, p. 108-18.

25. Van den Berg, L. and Pauly, S.W. "Recent Advances in Mercuric Iodide Detector Fabrication and Instrument Development," The Proceedings of SPIE, vol. 3769, 1999, p 203-10.

26. Van den Berg, L. and Vigil, R.D. "Fabrication of Mercuric Iodide Radiation Detectors," Nucl. Instr. and Meth., vol.A458, 2001, p. 148-51.

REPORT DOCUMENTATION PAGE

Form Approved
OMB No. 074-0188

1. REPORT DATE *(DD-MM-YYYY)*	2. REPORT TYPE	3. DATES COVERED *(From – To)*
09-03-2003	**Master's Thesis**	Jun 2002 – Mar 2003

4. TITLE AND SUBTITLE

DETECTION OF SPECIAL NUCLEAR MATERIALWITH HIGH PURITY GERMANIUM (HPGe) AND MERCURIC IODIDE (HgI_2) GAMMA DETECTORS

5a. CONTRACT NUMBER

5b. GRANT NUMBER

5c. PROGRAM ELEMENT NUMBER

6. AUTHOR(S)

Nelson, Michael B., Major, USA

5d. PROJECT NUMBER

5e. TASK NUMBER

5f. WORK UNIT NUMBER

7. PERFORMING ORGANIZATION NAMES(S) AND ADDRESS(S)

Air Force Institute of Technology
Graduate School of Engineering and Management (AFIT/EN)
2950 P Street, Building 640
WPAFB OH 45433-7765

8. PERFORMING ORGANIZATION REPORT NUMBER

AFIT/GNE/ENP/03-07

9. SPONSORING/MONITORING AGENCY NAME(S) AND ADDRESS(ES)

DTRA/TDAS
Attn: LTC Thomas Cartledge
8725 John J. Kingman Rd DSN: 221-9670
FT Belvoir, VA 22060-6201 e-mail: Thomas.Cartledge@DTRA.MIL

10. SPONSOR/MONITOR'S ACRONYM(S)

11. SPONSOR/MONITOR'S REPORT NUMBER(S)

12. DISTRIBUTION/AVAILABILITY STATEMENT

APPROVED FOR PUBLIC RELEASE; DISTRIBUTION UNLIMITED.

13. SUPPLEMENTARY NOTES

14. ABSTRACT

The Defense Threat Reduction Agency (DTRA) contracted for two gamma radiation detectors: mercuric iodide (HgI_2) and electromechanically cooled (EMC) high purity germanium (HPGe) to support arms control inspection efforts. This thesis investigated whether these detectors could measure the quality and quantity of special nuclear material (SNM), particularly Pu-239 for the treaty verification mission. The thesis investigated two areas of detector capabilities: 1) HgI_2 and HPGe detector performance necessary to characterize the quality of plutonium and the presence of shielding materials and 2) HgI_2 and EMC HPGe detector performance degradation by high noise levels and EMC HPGe detector performance degradation caused by electromechanical-cooling. The first area studied the response functions of each of the detectors necessary to meet the detection objectives: measure the Pu-239/Pu 240 ratio to identify weapons grade plutonium and to identify a phony weapon. The second area of detector performance evaluated was the EMC HPGe detector's cooling capabilities and its effect on the performance of the detector. The results show that neither of the detectors was ideally capable of supporting DTRA's requirements. The HgI_2 detector did not have sufficient efficiency or resolution to distinguish between Weapon Grade and Reactor Grade Plutonium. The EMC system suffered from grounding problems that degraded the resolution and efficiency. An initial study, evaluating the ability of detectors to determine the presence of a simulated tamper within the SNM physics package, showed great promise for identifying phony weapons.

15. SUBJECT TERMS

Mercuric Iodide, HgI_2, Special Nuclear Material, Spoof Identification, High Purity Germanium, HPGe, Electromechanically Cooled, EMC, Gamma Spectroscopy

16. SECURITY CLASSIFICATION OF:			17. LIMITATION OF ABSTRACT	18. NUMBER OF PAGES	19a. NAME OF RESPONSIBLE PERSON
a. REPORT	b. ABSTRACT	c. THIS PAGE			Larry W Burggraf, PhD, (ENP)
U	U	U	UU	126	19b. TELEPHONE NUMBER *(Include area code)* (937) 255-6565, ext 4507; e-mail: lburggra@afit.edu

Standard Form 298 (Rev. 8-98)
Prescribed by ANSI Std. Z39-18